

Inference of multiple high-dimensional networks with the Graphical Horseshoe prior

Claudio Busatto

Department of Statistics, Computer Science, Applications "G. Parenti",
University of Florence, Florence, Italy

and

Francesco Claudio Stingo

Department of Statistics, Computer Science, Applications "G. Parenti",
University of Florence, Florence, Italy

February 14, 2023

Abstract

We develop a novel full-Bayesian approach for multiple correlated precision matrices, called multiple Graphical Horseshoe (mGHS). The proposed approach relies on a novel multivariate shrinkage prior based on the Horseshoe prior that borrows strength and shares sparsity patterns across groups, improving posterior edge selection when the precision matrices are similar. On the other hand, there is no loss of performance when the groups are independent. Moreover, mGHS provides a similarity matrix estimate, useful for understanding network similarities across groups. We implement an efficient Metropolis-within-Gibbs for posterior inference; specifically, local variance parameters are updated via a novel and efficient modified rejection sampling algorithm that samples from a three-parameter Gamma distribution. The method scales well with respect to the number of variables and provides one of the fastest full-Bayesian approaches for the estimation of multiple precision matrices. Finally, edge selection is performed with a novel approach based on model cuts. We empirically demonstrate that mGHS outperforms competing approaches through both simulation studies and an application to a bike-sharing dataset.

Keywords: cuts-models, full-Bayesian inference, high-dimensional Gaussian graphical models, horseshoe priors, multiple graphical models, three-parameter Gamma distribution

1 Introduction

Graphical models are a popular tool used in many scientific fields to analyze and infer networks. In the Gaussian setting, the main challenges in graph estimation are the positive-definiteness con-

strain on precision matrices (inverse-covariance matrices) and the quadratic growth, with respect to the number of variables included in the analysis, of the number of free parameters. Traditional methods, such as the ones based on pairwise model comparisons, become computationally infeasible as the number of considered variables increases. For exchangeable observations, a collection of the existing methods for high-dimensional covariance matrix estimation is available in Pourahmadi (2011), in which the author proposes to reduce the problem to multiple independent (penalized) least-squares regressions. Other common approaches, such as the Graphical LASSO of Friedman et al. (2008) and the Graphical SCAD of Fan et al. (2009), are based on a penalized likelihood optimization and provide a sparse solution for the precision matrix in high-dimensional settings. A few approaches for the estimation of high-dimensional sparse networks have also been proposed within the Bayesian framework. In particular, the Bayesian version of the Graphical LASSO (Wang, 2012), the spike and slab stochastic search method (Wang, 2015), and the more recent Graphical Horseshoe presented in Li et al. (2019); all Bayesian methods implemented a block Gibbs sampler that has shown good computational performances up to a few hundred variables.

We are interested in settings where observations can be considered exchangeable only within groups; in these settings, a separate group-specific estimation will reduce the statistical power, while an analysis of data pooled across groups will lead to spurious findings (Peterson et al., 2015). Generalizations of the graphical models, called multiple graphical models, have been proposed with the aim of jointly estimating multiple correlated networks. Among the penalized likelihood approaches, the fused Graphical LASSO and the group Graphical LASSO of Danaher et al. (2014) rely on convex optimization problems and force similar edge values and similar graph structures, respectively. Bayesian approaches have been first proposed to encourage similar network structures across related subgroups (Peterson et al., 2015; Shaddox et al., 2018). More recent attempts, such as the generalization of the Bayesian spike and slab stochastic method of Peterson et al. (2020) and the GemBAG of Yang et al. (2021), focus on shared sparsity structures and precision matrix elements. See Ni et al. (2022) for a recent review of Bayesian approaches for complex graphical models, including methods for multiple groups.

Here we propose a generalization of the Graphical Horseshoe of Li et al. (2019) in the presence of multiple correlated sample groups, which we refer to as the *multiple Graphical Horseshoe* (mGHS). This model works under the multivariate Gaussianity assumption with multiple depen-

dent precision matrices. The proposed model is based on a novel prior on multiple covariance matrices that builds upon the Horseshoe prior proposed in Carvalho et al. (2010) and lets the data decide whether borrowing strength across groups and then encouraging similar precision matrices is appropriate. The properties of the Horseshoe prior are well-studied and include the improved Kullback-Leibler risk bound (Carvalho et al., 2010), minimaxity in estimation under the l_2 loss (Van der Pas et al., 2014) and improved risk properties in linear regression (Bhadra et al., 2016). Through simulation studies, we empirically show that the model benefits from the similar structures of the groups and provides better statistical performances than the Graphical Horseshoe applied separately to each group. The model relies on a Metropolis-within-Gibbs sampler where the parameters are updated by sampling from their full-conditional distributions and, in particular, a novel method is introduced in order to sample the local variance parameters. This method scales well with respect to the number of variables and is the first full Bayesian approach (to our knowledge) able to analyze multiple graphs of hundreds of nodes. Finally, we discuss a novel idea for posterior edge selection based on model cuts. The main novelties can be summarized as follow: 1) a novel shrinkage prior for multiple precision matrices, 2) an efficient algorithm that scales exceptionally well, and 3) a novel approach for edge selection based on model cuts.

The paper is organized as follows. In Section 2 the proposed sampling model is introduced. Section 3 illustrates how to sample from a three-parameters Gamma distribution (\mathcal{G}_{3p}) with a modified rejection sampling approach. Section 4 outlines the proposed algorithm in detail. In Section 5 we present a novel proposal for model selection. Section 6 illustrates comparative simulation studies, whereas in Section 7 we present an application to a benchmark bike-sharing dataset. Discussions and comments are presented in Section 8.

2 The model

In this section, we introduce the sampling model used to infer relationships among variables within each of K possibly related sample groups, each represented by a graph $G_k = (V, E_k)$, where V corresponds to a set of vertices and E_k to a set of group-specific edges. Let \mathbf{y}_{sk} be the p -dimensional random vector related to the observation s in group k , where $s = 1, \dots, n_k$ and $k = 1, \dots, K$.

Under the multivariate normal distribution, the corresponding sampling model is

$$\mathbf{y}_{sk} \sim \mathcal{N}_p(\mathbf{0}, \mathbf{\Sigma}_k),$$

where $\mathbf{\Omega}_k \equiv (\omega_{ij}^k)_{p \times p} = \mathbf{\Sigma}_k^{-1}$ is the precision matrix of group k . There is a one-to-one correspondence between the zero patterns in a precision matrix and an undirected graph G_k that, in turn, can be used to learn conditional independencies. Specifically, it can be shown that $\omega_{ij}^k = 0$ if and only if variables i and j are conditionally independent conditioning on the other variables (Dempster, 1972); in this case, the undirected graph G_k will have a missing edge between nodes i and j . Therefore, the goal is the joint estimation of non-zero entries in precision matrices with the aim of capturing significant connections among variables. In high-dimensional settings, the number of parameters to be estimated in $\mathbf{\Omega}_k$ is of order $O(p^2)$. This task is particularly challenging since these precision matrices, in addition to being very large, are constrained to the cone of symmetric positive definite matrices. Building upon the Graphical Horseshoe proposed by Li et al. (2019), we propose in Sections 2.1 and 4 model and algorithm, respectively, that use shrinkage priors to perform full Bayesian inference of multiple related high-dimensional undirected graphical models.

2.1 An horseshoe prior for multiple related precision matrices

Li et al. (2019) have successfully developed the Graphical Horseshoe prior, a shrinkage prior for (single) precision matrices. In this section, we describe how to extend the Graphical Horseshoe prior to multiple related precision matrices. The proposed approach will both achieve shrinkage and borrowing strength across related subgroups; as a key modeling feature, our approach will learn from the data which pairs of groups are related and which ones can be considered independent. With respect to the model proposed by Peterson et al. (2020), the only alternative full Bayesian approach that uses a joint prior on related multiple precision matrices, the proposed approach will result in a much more scalable algorithm, as detailed in Section 4.

Let $\boldsymbol{\omega}_{ij} = (\omega_{ij}^1, \dots, \omega_{ij}^K)^\top$ be the vector of precision matrix entries corresponding to edge (i, j) across K groups. Our approach builds upon the Graphical Horseshoe prior (Li et al., 2019), as we shrink non-informative edges ω_{ij}^k with a novel multivariate Horseshoe prior (Carvalho et al., 2010); we assume a non-informative prior for diagonal entries ω_{jj}^k . The joint prior distribution for

precision matrices $\boldsymbol{\Omega}_1, \dots, \boldsymbol{\Omega}_K$ can be written as

$$\begin{aligned} \pi(\omega_{jj}^k) &\propto 1, \quad k = 1, \dots, K, \quad j = 1, \dots, p \\ \pi(\boldsymbol{\Omega}_1, \dots, \boldsymbol{\Omega}_K | \boldsymbol{\Psi}_{ij} : i < j) &\propto \prod_{i < j} \mathcal{N}_K(\boldsymbol{\omega}_{ij} | \mathbf{0}, \boldsymbol{\Psi}_{ij}) \cdot \mathbb{I}_{(\boldsymbol{\Omega}_1, \dots, \boldsymbol{\Omega}_K \in \mathbb{M}_+^p)} \end{aligned}$$

where \mathbb{M}_+^p denotes the space of $p \times p$ positive-definite symmetric matrices. The proposed prior jointly models multiple precision matrices and, specifically, accounts for similarity between groups by imposing a K -variate normal prior distribution for $\boldsymbol{\omega}_{ij}$ with prior covariance matrix specific for each pair ij . As in Peterson et al. (2020), the proposed prior jointly learns both the within-group and across-group associations from the data in a single step, but it is computationally more efficient because it is based on continuous mixtures of multivariate normal distributions. Indeed, there is no need to sample the binary edge inclusion indicators as in Peterson et al. (2020).

Following the *separation strategy* introduced by Barnard et al. (2000), the across-group covariance matrices $\boldsymbol{\Psi}_{ij}$ can be decomposed as $\boldsymbol{\Psi}_{ij} = \boldsymbol{\Delta}_{ij} \mathbf{R} \boldsymbol{\Delta}_{ij}$, where $\boldsymbol{\Delta}_{ij} = \text{diag}\{\delta_{ij,1}, \dots, \delta_{ij,K}\}$ contains the standard deviations of edge (i, j) and $\mathbf{R} = \{r_{k'k} : k' < k\} \in \mathbb{M}_+^K$ is a valid correlation matrix with diagonal entries equal to one. As suggested by Barnard et al. (2000), we model variances $\delta_{ij,k}$ and correlations $r_{k'k}$ separately since it is generally not clear how these elements interact with each other. We apply the Horseshoe prior from Carvalho et al. (2010) by decomposing $\delta_{ij,k} = \tau_k \lambda_{ij,k}$ and imposing the following priors:

$$\lambda_{ij,k} \sim \mathcal{C}^+(0, 1), \tag{1}$$

$$\tau_k \sim \mathcal{C}^+(0, 1), \tag{2}$$

where \mathcal{C}^+ denotes the positive half-Cauchy distribution. In (1) and (2), parameters τ_k and $\lambda_{ij,k}$ control the global and local shrinkage of ω_{ij}^k , respectively. The heavy-tail distribution of $\lambda_{ij,k}$ allows ω_{ij}^k to avoid overshrinkage and lets the coefficients free to reach larger values. The amount of common shrinkage shared by the entries ω_{ij}^k is then controlled by the global scale parameter τ_k . When $K = 1$, the proposed model reduces to the Graphical Horseshoe of Li et al. (2019).

The selection of the prior distribution for correlation matrix \mathbf{R} is often more complicated. Barnard et al. (2000) give an overview of the most common prior for a correlation matrix. Here we follow Peterson et al. (2020) and choose the prior distribution

$$\pi(\mathbf{R}) \propto 1 \cdot \mathbb{I}_{(\mathbf{R} \in \mathbb{C}_+^K)},$$

where \mathbb{C}_+^K denotes the space of $K \times K$ definite-positive correlation matrices with diagonal entries equal to 1. The matrix \mathbf{R} allows the local variances λ_{ij}^k to share information between each other when the correlations between groups are large. On the contrary, the model reduces to the Graphical Horseshoe of Li et al. (2019) applied separately to each group when $\mathbf{R} = \mathbf{I}_K$ is the identity matrix. In Section 3 we introduce a new sampling algorithm for the three-parameter Gamma distribution that will be used within the algorithm for posterior inference detailed in Section 4.

3 The three-parameter Gamma $\mathcal{G}_{3p}(\gamma, \alpha, \beta)$ distribution and a modified rejection sampling algorithm

In this section, we introduce a modified acceptance-rejection method designed to generate samples from the three-parameter Gamma (\mathcal{G}_{3p}) distribution. Ahrens and Dieter (1982) and Stadlober (1982) demonstrated how to apply a rejection sampling for a target distribution when no valid proposal distribution is available. In particular, they proposed a modified rejection sampling to sample from a Gamma distribution and a t -Student distribution, respectively. Here the same situation applies since no trivial distribution, such as Gaussian or Gamma distributions, can be used as a valid proposal distribution. Indeed, it can be shown that these densities do not cover the target function on the latter's support, as required by the standard rejection sampling method. Therefore, we propose to overcome this problem by applying a modified rejection sampling with a Gaussian proposal distribution. The technical and theoretical aspects of this approach are detailed in Appendix A, where we also provide a proof that the method proposed in this section draws samples from the target distribution (3). For the sake of clarity, the notation used in this section does not relate to the notation used in the other sections.

Let $X \sim \mathcal{G}_{3p}(\gamma, \alpha, \beta)$, $\alpha, \beta \neq 0$, $\gamma \in \mathbb{N}^+$, a random variable with density

$$f_X(x | \gamma, \alpha, \beta) = \frac{e^{-\frac{\beta^2}{8\alpha^2}} (2\alpha^2)^{\frac{\gamma+1}{2}}}{\Gamma(\gamma+1) D_{-\gamma-1}\left(-\frac{\beta}{\alpha\sqrt{2}}\right)} x^\gamma e^{-\alpha^2 x^2 + \beta x} \cdot \mathbb{I}_{(x>0)}, \quad (3)$$

where $D_a(b)$ is the Parabolic Cylinder function with parameters a and b . The mean and variance

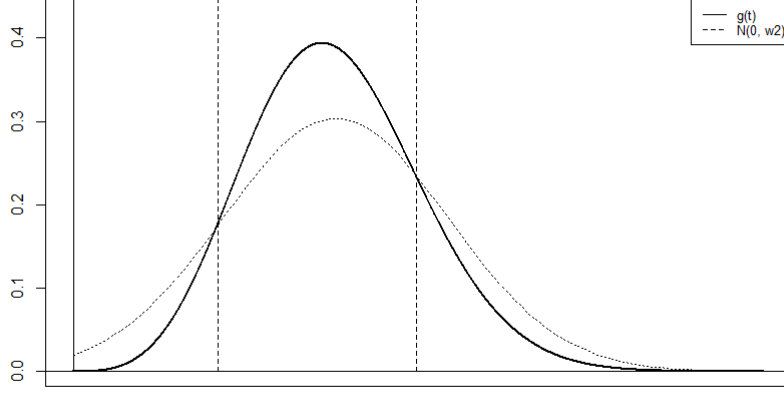


Figure 1: density g and h with $\gamma = 4$, $\alpha = 2.75$, $\beta = 3.3$; dotted lines represent t_1 and t_2 , whereas vertical line is the minimum $-\mu/\sigma$.

of variable X are

$$E(X) \equiv \mu = \frac{\gamma + 1}{\alpha\sqrt{2}} \frac{D_{-\gamma-2}\left(-\frac{\beta}{\alpha\sqrt{2}}\right)}{D_{-\gamma-1}\left(-\frac{\beta}{\alpha\sqrt{2}}\right)}$$

$$Var(X) \equiv \sigma^2 = \frac{(\gamma + 1)(\gamma + 2)}{2\alpha^2} \frac{D_{-\gamma-3}\left(-\frac{\beta}{\alpha\sqrt{2}}\right)}{D_{-\gamma-1}\left(-\frac{\beta}{\alpha\sqrt{2}}\right)} - \frac{(\gamma + 1)^2}{2\alpha^2} \frac{D_{-\gamma-2}\left(-\frac{\beta}{\alpha\sqrt{2}}\right)^2}{D_{-\gamma-1}\left(-\frac{\beta}{\alpha\sqrt{2}}\right)^2}.$$

The density $f(x) \sim \mathcal{G}_{3p}(\gamma, \alpha, \beta)$ is transformed into a standardized distribution $g(t) = \sigma f(\sigma t + \mu)$ by the transformation $t = (x - \mu)/\sigma$, with support on the interval $(-\frac{\mu}{\sigma}, \infty)$. A new value t_* can be drawn from $g(t)$ using the modified rejection sampling described below. Finally, the value $x_* = \sigma t_* + \mu$ is returned.

Consider the proposal distribution $h(t) \sim \mathcal{N}(0, \omega^2)$ and the ratio

$$\begin{aligned} r(t_*) &= \frac{g(t_*)}{h(t_*)} = \frac{\sigma f(\sigma t_* + \mu)}{h(t_*)} \\ &= \omega\sigma C_f \sqrt{2\pi} (\sigma t_* + \mu)^\gamma e^{-\alpha^2(\sigma t_* + \mu)^2 + \beta(\sigma t_* + \mu) - \frac{t_*^2}{2\omega^2}} \cdot \mathbb{I}_{(t_* > -\frac{\mu}{\sigma})} \\ &= \omega\sigma C_f \sqrt{2\pi} (\sigma t_* + \mu)^\gamma e^{(\frac{1}{2\omega^2} - \alpha^2\sigma^2)t_*^2 + (\beta - 2\mu\alpha^2)\sigma t_* + \beta\mu - \alpha^2\mu^2}, \end{aligned} \quad (4)$$

where C_f is the normalizing constant of $f(x)$ and $(\beta - 2\mu\alpha^2) < 0$. The analysis of $r(t)$ gives insights on how to correctly choose the variance ω^2 of the proposal distribution $h(t)$, as $r(t)$

needs to be bounded and should go to zero as t increases. For this reason we set the variance to $w^2 = \frac{1}{2\alpha^2\sigma^2}$ and the ratio in (4) evaluated at t_* can be re-written as

$$r(t_*) = \omega\sigma C_f \sqrt{2\pi} (\sigma t_* + \mu)^\gamma e^{(\beta - 2\mu\alpha^2)(\sigma t_* + \mu) + \alpha^2\mu^2},$$

which is analytically tractable. In order to apply a standard rejection sampling, the method requires that $r(t_*) \leq 1$. However, as shown in Figure 1, the proposal density $h(t)$ lays below the target density $g(t)$ in the interval $[t_1, t_2]$, with

$$t_1 = \frac{\gamma}{\sigma(\beta - 2\mu\alpha^2)} W_0 \left(\frac{(\beta - 2\mu\alpha^2)}{\gamma} \left(\frac{e^{-\alpha^2\mu^2}}{\omega\sigma C_f \sqrt{2\pi}} \right)^{\frac{1}{\gamma}} \right) - \frac{\mu}{\sigma},$$

$$t_2 = \frac{\gamma}{\sigma(\beta - 2\mu\alpha^2)} W_{-1} \left(\frac{(\beta - 2\mu\alpha^2)}{\gamma} \left(\frac{e^{-\alpha^2\mu^2}}{\omega\sigma C_f \sqrt{2\pi}} \right)^{\frac{1}{\gamma}} \right) - \frac{\mu}{\sigma},$$

where W denotes the Lambert function. It can be analytically shown that $r(t_{max}) \geq 1$, where $t_{max} = -\frac{\gamma}{\sigma(\beta - 2\mu\alpha^2)} - \frac{\mu}{\sigma}$ is the global maximum of the ratio. Therefore, a standard rejection sampling cannot be applied. Noting that in the intervals $(-\frac{\mu}{\sigma}, t_1)$ and (t_2, ∞) it yields $h(t) > g(t)$, the rejection sampling algorithm can be modified as follows:

- Step 1: generate a sample t_* from $h(t)$ and immediately accept $x_* = \sigma t_* + \mu$ if $t_1 \leq t_* \leq t_2$;
- Step 2: if $t_* < t_1$ or $t_* > t_2$, generate a sample u from a $\mathcal{U}(0, 1)$ density and compute $r(t_*)$. Accept $x_* = \sigma t_* + \mu$ if $u \leq r(t_*)$. The computation of $r(t_*)$ can often be avoided if an accurate lower bound for the tails of the ratio is available;
- Step 3: if Step 2 leads to rejection, take a new sample t'_* from the distribution $d(t) = g(t) - h(t)$, in the interval $[t_1, t_2]$ and return $x'_* = \sigma t'_* + \mu$. Sampling from $d(t)$ can be achieved by means of a standard rejection sampling, as in Ahrens and Dieter (1982), Stadlober (1982). More details about this step can be found in Appendix A.2.

The acceptance probability of each step is discussed in Appendix A.1.

Proposition 3.1. *The modified rejection sampling defined by steps 1, 2, and 3 draws a sample from a \mathcal{G}_{3p} distribution with probability 1.*

Proof See Appendix A.3.

The main computational bottleneck of the method is the evaluation of the Parabolic Cylinder function D . This issue can be alleviated by exploiting the following proposition and by the application of sharp approximations.

Proposition 3.2. *The Kullback-Leibler divergence (KL) between a distribution $q_x \sim \mathcal{G}_{3p}(\gamma, \alpha, \beta)$ and a distribution $p_x \sim \mathcal{G}(d, c)$, where $d = \gamma + 1$ and $c = -\beta$, goes to zero when $\beta/\alpha \rightarrow -\infty$.*

Proof See Appendix B.

Furthermore, when $\beta/\alpha \rightarrow \infty$ or $\gamma \rightarrow \infty$, the three-parameter Gamma distribution can be conveniently approximated by a Normal distribution. We empirically show that, in these cases, the KL divergence between a distribution $q_x \sim \mathcal{G}_{3p}(\gamma, \alpha, \beta)$ and a distribution $p_x \sim \mathcal{N}(m, s^2)$ asymptotically goes to 0, where estimates of m and s^2 are given in Appendix B. These empirical results, along with proposition 3.2, can be used to efficiently evaluate the mean and variance of the target distribution without the need to compute the function D for some combinations of the parameters' value.

4 Posterior sampling

We develop an efficient MCMC algorithm to sample from the posterior distribution of the parameters. The algorithm can be divided into three main steps: 1. a Gibbs step for the update of parameters $\boldsymbol{\Omega}_1, \dots, \boldsymbol{\Omega}_K$; 2. a Gibbs step for the update of shrinkage parameters $\boldsymbol{\Lambda}_1^2, \dots, \boldsymbol{\Lambda}_K^2$ and $\boldsymbol{\tau}^2$; 3. a Metropolis-Hastings (MH) step for the update of correlation matrix \mathbf{R} . In step 2 we make use of the modified rejection sampler introduced in Section 3. The complete algorithm is shown in Appendix A of Supplementary Materials.

1. Sampling $\boldsymbol{\Omega}_1, \dots, \boldsymbol{\Omega}_K$. The full conditional distribution of $\boldsymbol{\Omega}_1, \dots, \boldsymbol{\Omega}_K$ is

$$\pi(\boldsymbol{\Omega}_1, \dots, \boldsymbol{\Omega}_K | \cdot) \propto \prod_{k=1}^K |\boldsymbol{\Omega}_k|^{\frac{n_k}{2}} \exp \left\{ -\frac{1}{2} \text{tr}(\mathbf{S}_k \boldsymbol{\Omega}_k) \right\} \cdot \prod_{i < j} \exp \left\{ -\frac{1}{2} \boldsymbol{\omega}_{ij}^\top \boldsymbol{\Delta}_{ij}^{-1} \mathbf{R}^{-1} \boldsymbol{\Delta}_{ij}^{-1} \boldsymbol{\omega}_{ij} \right\} \cdot \mathbb{I}_{(\boldsymbol{\Omega}_1, \dots, \boldsymbol{\Omega}_K \in \mathbb{M}_+^K)}$$

where $\mathbf{S}_k = \sum_{s=1}^{n_k} \mathbf{y}_{sk} \mathbf{y}_{sk}^\top$ and $tr(\cdot)$ denotes the trace. Precision matrices $\boldsymbol{\Omega}_1, \dots, \boldsymbol{\Omega}_K$ can be updated by adapting the block Gibbs sampler proposed in Wang (2015) for the estimation of a single precision matrix. Following Peterson et al. (2020), for each sample group $k = 1, \dots, K$ precision matrix $\boldsymbol{\Omega}_k$ is updated column-wise by sampling from the full-conditional distribution of each column $j = 1, \dots, p$ conditionally on both the rest of the columns of group k and on the j -th column of the remaining $k - 1$ sample groups. Consider the following partition of vector $\boldsymbol{\omega}_{ij}$ and matrices $\boldsymbol{\Delta}_{ij}$ and \mathbf{R} :

$$\boldsymbol{\omega}_{ij} = \begin{bmatrix} \boldsymbol{\omega}_{ij}^{-k} \\ \boldsymbol{\omega}_{ij}^k \end{bmatrix}, \quad \boldsymbol{\Delta}_{ij} = \begin{bmatrix} \boldsymbol{\Delta}_{ij,-k} & \mathbf{0} \\ \mathbf{0}^\top & \delta_{ij,k} \end{bmatrix} \quad \text{and} \quad \mathbf{R} = \begin{bmatrix} \mathbf{R}_{-k} & \mathbf{r}_k \\ \mathbf{r}_k^\top & 1 \end{bmatrix}. \quad (5)$$

The full conditional of $\boldsymbol{\Omega}_k$ is:

$$\pi(\boldsymbol{\Omega}_k | \cdot) \propto |\boldsymbol{\Omega}_k|^{\frac{n_k}{2}} \exp \left\{ -\frac{1}{2} tr(\mathbf{S}_k \boldsymbol{\Omega}_k) \right\} \prod_{i < j} \exp \left\{ -\frac{1}{2d_{ij}^k} (\boldsymbol{\omega}_{ij}^k - \delta_{ij,k} \mathbf{r}_k^\top \mathbf{R}_{-k}^{-1} \boldsymbol{\Delta}_{ij,-k}^{-1} \boldsymbol{\omega}_{ij}^{-k})^2 \right\}, \quad (6)$$

where $d_{ij}^k = \delta_{ij,k}^2 (1 - \mathbf{r}_k^\top \mathbf{R}_{-k}^{-1} \mathbf{r}_k)$. As proposed in Wang (2015), sampling from (6) can be achieved by updating one column of $\boldsymbol{\Omega}_k$ at the time. Without loss of generality, consider the permutation of the columns such that the j -th column becomes the last one. This permutation leads to the following partition:

$$\mathbf{S}_k = \begin{bmatrix} \mathbf{S}_{-j}^k & \mathbf{s}_j^k \\ (\mathbf{s}_j^k)^\top & s_{jj}^k \end{bmatrix} \quad \text{and} \quad \boldsymbol{\Omega}_k = \begin{bmatrix} \boldsymbol{\Omega}_{-j}^k & \boldsymbol{\omega}_j^k \\ (\boldsymbol{\omega}_j^k)^\top & \omega_{jj}^k \end{bmatrix}.$$

The full-conditional distribution of parameters $(\omega_{jj}^k, \boldsymbol{\omega}_j^k)$ is

$$\pi(\omega_{jj}^k, \boldsymbol{\omega}_j^k | \cdot) \propto \left(\omega_{jj}^k - (\boldsymbol{\omega}_j^k)^\top (\boldsymbol{\Omega}_{-j}^k)^{-1} \boldsymbol{\omega}_j^k \right)^{\frac{n_k}{2}} \cdot e^{-\frac{1}{2} ((\boldsymbol{\omega}_j^k - \mathbf{m}_{j,k})^\top \mathbf{D}_{j,k}^{-1} (\boldsymbol{\omega}_j^k - \mathbf{m}_{j,k}) + 2(\boldsymbol{\omega}_j^k)^\top \mathbf{s}_{j+k}^k + s_{jj}^k \omega_{jj}^k)}, \quad (7)$$

where $\mathbf{m}_{j,k}$ is the $(p-1)$ -dimensional vector with entries $m_{j,k}^i = \delta_{ij,k} \mathbf{r}_k^\top \mathbf{R}_{-k}^{-1} \boldsymbol{\Delta}_{ij,-k}^{-1} \boldsymbol{\omega}_{ij}^{-k}$ and $\mathbf{D}_{j,k}$ is diagonal with entries d_{ij}^k , $i = 0, \dots, p, i \neq j$. A closed form for sampling from (7) can be obtained with the transformation $(\mathbf{v}_{j,k}, \gamma_{jj}^k) \rightarrow (\boldsymbol{\omega}_j^k, \omega_{jj}^k - (\boldsymbol{\omega}_j^k)^\top (\boldsymbol{\Omega}_{-j}^k)^{-1} \boldsymbol{\omega}_j^k)$, which yields

$$\gamma_{jj}^k | \cdot \sim \mathcal{G} \left(\frac{n_k}{2} + 1, \frac{s_{jj}^k}{2} \right),$$

$$\mathbf{v}_{j,k} | \cdot \sim \mathcal{N}_{p-1} \left(\boldsymbol{\Sigma}_{j,k}^{-1} (\mathbf{D}_{j,k}^{-1} \mathbf{m}_{j,k} - \mathbf{s}_{jj}^k), \boldsymbol{\Sigma}_{j,k}^{-1} \right)$$

where \mathcal{G} denotes the Gamma distribution and $\Sigma_{j,k} = \mathbf{D}_{j,k}^{-1} + s_{jj}^k (\mathbf{\Omega}_{-j}^k)^{-1}$. Therefore, values ω_{jj}^k and ω_j^k can be updated by first sampling γ_{jj}^k and $\mathbf{v}_{j,k}$ and then applying the inverse transformation.

Computationally, this is the most expensive step of the algorithm due to the need to invert the matrices $\mathbf{\Omega}_{-j}^k$ and $\Sigma_{j,k}$. In our implementation of the Gibbs steps for γ_{jj}^k and $\mathbf{v}_{j,k}$, we make use of Sherman-Morrison formula to update $(\mathbf{\Omega}_{-j}^k)^{-1}$ with $O(p^2)$ operations, instead of $O(p^3)$.

2. Sampling $\Lambda_1^2, \dots, \Lambda_K^2$ and τ^2 . Samplers commonly used in conjunction with Horseshoe prior cannot be implemented for the proposed model. Indeed, the positive half-Cauchy distribution is not conjugated to the variance in a multivariate normal means model. Our approach builds upon the data-augmentation scheme proposed Makalic and Schmidt (2016). We introduce the auxiliary variables $\eta_{ij,k}$ and ζ_k such that

- if $\lambda_{ij,k}^2 \mid \eta_{ij,k} \sim \mathcal{IG}\left(\frac{1}{2}, \frac{1}{\eta_{ij,k}}\right)$ and $\eta_{ij,k} \sim \mathcal{IG}\left(\frac{1}{2}, 1\right)$, then $\lambda_{ij,k} \sim \mathcal{C}^+(0, 1)$;
- if $\tau_k^2 \mid \zeta_k \sim \mathcal{IG}\left(\frac{1}{2}, \frac{1}{\zeta_k}\right)$ and $\zeta_k \sim \mathcal{IG}\left(\frac{1}{2}, 1\right)$, then $\tau_k \sim \mathcal{C}^+(0, 1)$.

After conditioning on the auxiliary variables $\eta_{ij,k}$ and ζ_k , the full conditional distribution of parameters $\mathbf{\Lambda}$ and $\boldsymbol{\tau}$ can be written as

$$\begin{aligned} \pi(\mathbf{\Lambda}, \boldsymbol{\tau} \mid \cdot) &\propto \prod_{i < j} |\Delta_{ij}|^{-1} \exp\left\{-\frac{1}{2} \boldsymbol{\omega}_{ij}^\top (\Delta_{ij} \mathbf{R} \Delta_{ij})^{-1} \boldsymbol{\omega}_{ij}\right\} \\ &\quad \prod_{k=1}^K \tau_k^{-3} \exp\left\{-\frac{1}{\zeta_k \tau_k^2}\right\} \cdot \prod_{i < j} \lambda_{ij,k}^{-3} \exp\left\{-\frac{1}{\eta_{ij,k} \lambda_{ij,k}^2}\right\}. \end{aligned}$$

Local shrinkage matrix $\mathbf{\Lambda}_k$ is updated column-wise alongside precision matrix $\mathbf{\Omega}_k$. Considering the partition of $\boldsymbol{\omega}_{ij}$, Δ_{ij} and \mathbf{R} in (5), the full-conditionals of parameters $\lambda_{ij,k}^2$ and τ_k^2 related to group k are

$$\begin{aligned} \pi(\lambda_{ij,k}^2 \mid \cdot) &\propto \lambda_{ij,k}^{-4} \exp\left\{-\frac{\alpha_{\lambda_{ij,k}}}{\lambda_{ij,k}^2} + \frac{\beta_{\lambda_{ij,k}}}{\lambda_{ij,k}}\right\} \cdot \mathbb{I}(\lambda_{ij,k}^2 > 0), \\ \alpha_{\lambda_{ij,k}} &= \frac{1}{\eta_{ij,k}} + \frac{(\omega_{ij}^k)^2}{2\tau_k^2 \mu_k} \quad \text{and} \quad \beta_{\lambda_{ij,k}} = \frac{\omega_{ij}^k}{\tau_k \mu_k} \mathbf{r}_k^\top \mathbf{R}_{-k}^{-1} \Delta_{ij,-k}^{-1} \boldsymbol{\omega}_{ij}^{-k}, \end{aligned} \quad (8)$$

$$\begin{aligned} \pi(\tau_k^2 \mid \cdot) &\propto \tau_k^{-\frac{p(p-1)}{2}-3} \exp\left\{-\frac{\alpha_{\tau_k}}{\tau_k^2} + \frac{\beta_{\tau_k}}{\tau_k}\right\} \cdot \mathbb{I}(\tau_k^2 > 0), \\ \alpha_{\tau_k} &= \frac{1}{\zeta_k} + \frac{1}{2} \sum_{i < j} \frac{(\omega_{ij}^k)^2}{\lambda_{ij,k}^2 \mu_k} \quad \text{and} \quad \beta_{\tau_k} = \sum_{i < j} \frac{\omega_{ij}^k}{\lambda_{ij,k} \mu_k} \mathbf{r}_k^\top \mathbf{R}_{-k}^{-1} \Delta_{ij,-k}^{-1} \boldsymbol{\omega}_{ij}^{-k} \end{aligned} \quad (9)$$

where $\mu_k = 1 - \mathbf{r}_k^\top \mathbf{R}_{-k}^{-1} \mathbf{r}_k$. Note that the full conditional distributions show a shared amount of global and local shrinkage, as the model exploits the similarity among groups and learns from the structures of the other graphs. Densities (8) and (9) are a transformation of \mathcal{G}_{3p} random variables introduced in Section 3. Specifically,

$$\begin{aligned} \text{if } u &\sim \mathcal{G}_{3p}(1, \alpha_{\lambda_{ij,k}}, \beta_{\lambda_{ij,k}}), & \text{then } \lambda_{ij,k}^2 &= 1/u^2, \\ \text{if } u &\sim \mathcal{G}_{3p}(p(p-1)/2, \alpha_{\tau_k}, \beta_{\tau_k}), & \text{then } \tau_k^2 &= 1/u^2. \end{aligned}$$

We use the sampling algorithm introduced in Section 3 to efficiently obtain samples from these distributions. Finally, hyper-parameters $\eta_{ij,k}$ and ζ_k are updated by sampling from the inverse-Gamma distributions $\eta_{ij,k} \sim \mathcal{IG}(1, 1 + 1/\lambda_{ij,k}^2)$ and $\zeta_k \sim \mathcal{IG}(1, 1 + 1/\tau_k^2)$.

3. Sampling \mathbf{R} . The similarity among groups is captured through correlation matrix $\mathbf{R} \in \mathbb{C}_+^K$. Following Peterson et al. (2020), we implement a modified version of the Metropolis-Hastings sampler proposed by Liu and Daniels (2006), which relies on a candidate prior distribution $\pi^*(\mathbf{R})$ that is used to define a proposal distribution for correlation matrices. In the first step of this data-augmentation approach a $K \times K$ covariance matrix Θ is sampled from an Inverse-Wishart distribution; in the second step, a reduction function is applied to map the covariance matrix to a valid correlation matrix, that is eventually accepted with an MH step.

We introduce a diagonal matrix \mathbf{V} such that $\Theta = \mathbf{V}\mathbf{R}\mathbf{V}$; the matrix \mathbf{V} maps the correlation matrix \mathbf{R} to the covariance matrix Θ . Following Peterson et al. (2020), the transformation from the standard parameter space to the expanded space is achieved as

$$\boldsymbol{\omega}_{ij} = \mathbf{V}^{-1} \boldsymbol{\epsilon}_{ij}, \quad \mathbf{R} = \mathbf{V}^{-1} \Theta \mathbf{V}^{-1}, \quad (10)$$

where $\sum_{i < j} \epsilon_{ijk}^2 = 1$, for $k = 1, \dots, K$ and $\mathbf{V} = \text{diag} \left\{ \sum_{i < j} (\omega_{ij}^1)^2, \dots, \sum_{i < j} (\omega_{ij}^K)^2 \right\}$. Let the candidate prior distribution be

$$\pi^*(\mathbf{R}) \propto |\mathbf{R}|^{-\frac{K+1}{2}} \cdot \mathbb{I}_{(\mathbf{R} \in \mathbb{C}_+^K)}, \quad (11)$$

then the proposal density for matrix \mathbf{R} is

$$\begin{aligned} q(\mathbf{R} | \cdot) &\propto \pi^*(\mathbf{R}) \cdot \pi(\boldsymbol{\Omega}_1, \dots, \boldsymbol{\Omega}_K | \mathbf{R}) \\ &\propto |\mathbf{R}|^{-\frac{K+1+p(p-1)/2}{2}} \cdot \prod_{i < j} e^{-\frac{1}{2} \boldsymbol{\omega}_{ij}^\top \boldsymbol{\Delta}_{ij}^{-1} \mathbf{R}^{-1} \boldsymbol{\Delta}_{ij}^{-1} \boldsymbol{\omega}_{ij}}, \end{aligned}$$

which is conditioned on the current state of the algorithm and accounts for the dependency with parameters $\boldsymbol{\Omega}_1, \dots, \boldsymbol{\Omega}_K$, $\boldsymbol{\Lambda}_1, \dots, \boldsymbol{\Lambda}_K$ and $\boldsymbol{\tau}^2$. Note that (11) concentrates its mass around zero when K increases; for this reason, a reasonably small number of sample groups K is required. The Jacobian of the transformation defined in (10) is $J = |\mathbf{V}^{-1}|^{\frac{p(p-1)}{2} + K + 1}$, thus the proposal distribution for the MH sampler is

$$\begin{aligned} q(\boldsymbol{\Theta} \mid \cdot) &\propto \pi^*(\boldsymbol{\Theta}) \cdot \pi(\boldsymbol{\Omega}_1, \dots, \boldsymbol{\Omega}_K \mid \boldsymbol{\Theta}) \\ &\propto |\boldsymbol{\Theta}|^{-\frac{K+1+p(p-1)/2}{2}} e^{-\frac{1}{2} \sum_{i < j} \boldsymbol{\epsilon}_{ij}^T \boldsymbol{\Delta}_{ij}^{-1} \boldsymbol{\Theta}^{-1} \boldsymbol{\Delta}_{ij}^{-1} \boldsymbol{\epsilon}_{ij}} \end{aligned} \quad (12)$$

which is a $\mathcal{IW}\left(\frac{p(p-1)}{2}, \mathbf{H}\right)$, where $\mathbf{H} = \sum_{i < j} \boldsymbol{\Delta}_{ij}^{-1} \boldsymbol{\epsilon}_{ij} \boldsymbol{\epsilon}_{ij}^T \boldsymbol{\Delta}_{ij}^{-1}$. Therefore, a candidate $\boldsymbol{\Theta}^*$ is sampled from (12) and then mapped to \mathbf{R}^* via the inverse transformation $\mathbf{R}^* = \mathbf{V}^{-1} \boldsymbol{\Theta}^* \mathbf{V}^{-1}$. New correlation matrix \mathbf{R}^* is accepted with probability

$$\begin{aligned} \alpha &= \min \left\{ 1, \frac{\pi(\mathbf{R}^* \mid \cdot) \cdot q(\mathbf{R} \mid \cdot)}{\pi(\mathbf{R} \mid \cdot) \cdot q(\mathbf{R}^* \mid \cdot)} \right\} \\ &= \min \left\{ 1, e^{\frac{K+1}{2} (\log |\mathbf{R}^*| - \log |\mathbf{R}|)} \right\}, \end{aligned}$$

where $p(\mathbf{R} \mid \cdot) \propto \pi(\mathbf{R}) \cdot \pi(\boldsymbol{\Omega}_1, \dots, \boldsymbol{\Omega}_K \mid \mathbf{R})$ denotes the full-conditional distribution of \mathbf{R} .

5 Posterior edge selection

A practical problem with continuous shrinkage priors is model selection since the parameters are shrunk toward zero but never exactly zero. A common method relies on posterior marginal credible intervals. However, Van der Pas et al. (2017) have shown that under the Horseshoe prior in a Normal means problem, this method leads to a conservative variables selection procedure where some of the zero parameters are falsely selected, whereas some signal is not, due to wide intervals for non-zero parameters. To avoid such a problem, Li et al. (2019) used 50% credible intervals to control the number of false negatives. This choice is in line with the *median probability model* (MPM) of Barbieri and Berger (2004). The MPM model is defined as the model that includes only those edges with marginal posterior probability greater (or equal) than 1/2. In the context of linear regression models, Barbieri and Berger (2004) have shown that this method represents the predictive optimal model under some common but strict hypothesis, such as orthogonality of the covariates. The result is extended to g -type spike and slab priors in Barbieri et al. (2021). This

approach is used, among many others, in Wang (2015) and Peterson et al. (2020). A practical example of an MPM-like strategy can be found in Carvalho et al. (2010). The authors show that the Horseshoe estimator is $\beta_j^{\text{HS}} = \lambda_j^2 / (1 + \lambda_j^2) \beta_j^{\text{OLS}}$, where λ_j^2 and β_j denote the local shrinkage parameter and the regression parameter of variable j , respectively, and propose to set to zero those variables for which $\lambda_j^2 / (1 + \lambda_j^2) < 1/2$.

The cited methods present two main drawbacks. First, the optimality results in Barbieri and Berger (2004) only hold for fixed design $\tilde{\mathbf{X}}$ of prediction point or for stochastic predictors with $\mathbb{E}(\tilde{\mathbf{X}}^\top \tilde{\mathbf{X}})$, which are often unrealistic assumptions; therefore, the threshold 1/2 does not ensure the optimality of the selected model under the considered framework, where the goal is to analyze the connections between variables. Secondly, the considered selection procedures rely on marginal values and do not account for any posterior correlation among the parameters.

To overcome these problems, we propose a “quasi-bayesian” approach for edge selection that accounts for the posterior dependencies among the parameters. The method relies on a *cut* function that “cuts” the relationship between the parameters to prevent model feedback which could negatively affect the performances of the model (Zigler et al., 2013; Plummer, 2015). Cuts have been used in different contexts (Lunn et al., 2009; Bayarri et al., 2009; McCandless et al., 2010; Blangiardo et al., 2011; Zigler, 2016) either to control the flow of information or to gain a computational advantage. Bayarri et al. (2009) consider the cut function as a “*modularization*” of the model. This approach breaks a bigger model into smaller parts called modules, modifying the magnitude of the interactions between the parameters in different modules.

5.1 An extended model and algorithm for edge selection

In this section, we extend the model presented in the previous sections introducing two parameters t_α and \mathbf{z} , and an algorithm that updates these parameters with a Metropolis-within-Gibbs step. Notation refers to a single graph and can be easily extended to the case of multiple graphs.

The parameter $t_\alpha \in (0, 1)$ can be interpreted as a threshold for edge selection, and the latent variable \mathbf{z} is a $p(p-1)/2$ -binary vector with generic element $z_{ij} = 1$ if the corresponding edge ω_{ij} , $i < j$, is included in the model, $z_{ij} = 0$ otherwise. Formally, the model is defined as

$$z_{ij} = 1 \text{ if } \kappa_{ij} \geq t_\alpha, \text{ and } z_{ij} = 0 \text{ otherwise,}$$

where $\kappa_{ij} = \lambda_{ij}^2 / (1 + \lambda_{ij}^2)$. Here the goal is to estimate parameter t_α based on the posterior values

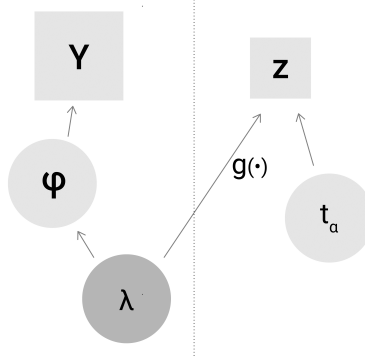


Figure 2: Graphical representation of the model. The dotted line denotes the cut function, stopping the flows of information from \mathbf{z} to $\boldsymbol{\lambda}$.

of $\boldsymbol{\lambda}$. At the same time, we want to prevent the flow of information from t_α and \mathbf{z} to $\boldsymbol{\lambda}$. The cut function comes in handy to avoid such issues. The modularization of the proposed model is shown in Figure 2, where $\boldsymbol{\varphi} = (\boldsymbol{\Omega}, \boldsymbol{\tau}, \mathbf{R})$ and parameters \mathbf{z} and $\boldsymbol{\lambda}$ are connected through the reparametrization κ_{ij} .

Different prior distributions can be assumed for t_α ; a natural choice is $t^\alpha \sim \text{Beta}(a, b)$. Parameters z_{ij} can be seen as the realization of $p(p-1)/2$ Bernoulli distributions $z_{ij} \mid \kappa_{ij}, \boldsymbol{\varphi}, t_\alpha \sim \text{Ber}(q_{ij}^\alpha)$, where $q_{ij}^\alpha = 1 - \mathbb{P}(\kappa_{ij} \leq t^\alpha \mid \boldsymbol{\varphi})$. The joint likelihood of the model can be factorized as

$$\begin{aligned} \pi(\mathbf{Y}, \boldsymbol{\lambda}, \boldsymbol{\varphi}, \mathbf{z}, t_\alpha) &\propto \pi(\boldsymbol{\varphi} \mid \mathbf{Y}, \boldsymbol{\lambda}) \pi(\mathbf{z}, t_\alpha \mid \boldsymbol{\kappa}, \boldsymbol{\varphi}) \pi(\boldsymbol{\lambda}), \\ &\propto \pi(\boldsymbol{\lambda}, \boldsymbol{\varphi} \mid \mathbf{Y}) \pi(\mathbf{z}, t_\alpha \mid \boldsymbol{\kappa}, \boldsymbol{\varphi}). \end{aligned}$$

The modularization of the model allows us to sample directly from the conditional distributions $\pi(\boldsymbol{\lambda}, \boldsymbol{\varphi} \mid \mathbf{Y})$ and $\pi(\mathbf{z}, t_\alpha \mid \boldsymbol{\kappa}, \boldsymbol{\varphi})$, thus evaluating parameters $\boldsymbol{\lambda}$ and $\boldsymbol{\varphi}$ without the influence of the unknown quantity \mathbf{z} . The joint posterior distribution of parameters t_α and \mathbf{z} is

$$\pi(\mathbf{z}, t^\alpha \mid \boldsymbol{\kappa}, \boldsymbol{\varphi}) \propto (t^\alpha)^{a-1} (1 - t^\alpha)^{b-1} \cdot \prod_{j=1}^p \prod_{i < j} (q_{ij}^\alpha)^{z_{ij}} (1 - q_{ij}^\alpha)^{1-z_{ij}}. \quad (13)$$

We propose a Metropolis-within-Gibbs algorithm in order to sample from (13). Parameters z_{ij} are sampled from the full-conditional distribution

$$z_{ij} \mid \kappa_{ij}, \boldsymbol{\varphi}, t^\alpha \sim \text{Ber}(q_{ij}^\alpha).$$

Under the framework introduced in Section 4, the transformation $\kappa_{ij} = \lambda_{ij}^2 / (1 + \lambda_{ij}^2)$ with Jaco-

bian $J_{\kappa_{ij}} = (1 + \kappa_{ij})^{-2}$ yields

$$\pi(\kappa_{ij} \mid \mathbf{Y}, \boldsymbol{\varphi}) \propto \kappa_{ij}^{-2} \exp \left\{ -\alpha_{\lambda_{ij}} \frac{1 - \kappa_{ij}}{\kappa_{ij}} + \beta_{\lambda_{ij}} \sqrt{\frac{1 - \kappa_{ij}}{\kappa_{ij}}} \right\} \cdot \mathbb{I}_{(\kappa_{ij} \in (0,1))},$$

where the cumulative density function $F_{\kappa_{ij} \mid \mathbf{Y}, \boldsymbol{\varphi}}(t^\alpha)$ is available in closed form. Therefore, the quantity q_{ij}^α can be analytically and efficiently computed conditionally on the current state of $\boldsymbol{\varphi}$.

The threshold t^α is then updated with a MH step, where the new values t_*^α are sampled from the prior distribution. The acceptance probability of this step is

$$\alpha_{\text{MH}} = \min \left\{ 1, \frac{\pi(\mathbf{z}, t_*^\alpha \mid \boldsymbol{\kappa}, \boldsymbol{\varphi})}{\pi(\mathbf{z}, t^\alpha \mid \boldsymbol{\kappa}, \boldsymbol{\varphi})} \right\}.$$

The sampled values of t^α can be used to perform graph selection; specifically, we include in the graph all edges such that $P(\kappa_{ij} \mid \mathbf{Y}, \boldsymbol{\varphi}) > t^\alpha$. Hereafter, we consider both this approach and the MPM method ($t^\alpha = 1/2$; Carvalho et al., 2010) as two alternative approaches to posterior edge selection.

6 Simulation studies

We perform simulation studies that cover several scenarios of interest. The performances of the proposed model and competing approaches are tested in four scenarios all comprising $K = 4$ groups:

- **Independence set-up:** the groups are simulated from multivariate Gaussian distributions with a different precision matrix for each group;
- **Coupled set-up:** each pair of groups is simulated from a multivariate Gaussian distribution with the same precision matrix;
- **P2020 set-up:** the groups are simulated following the scheme of Peterson et al. (2020), where each precision matrix is created by adding (deleting) new edges to (from) the other precision matrices;
- **Full-dependence set-up:** the groups are simulated from multivariate Gaussian distributions with equal precision matrices.

The precision matrices are simulated following the approach of Peterson et al. (2020), which relies on a generalization of the method proposed by Danaher et al. (2014). Edges are divided into independent subgroups with size either equal to 5 or 10. Diagonal entries of the precision matrices are set to 1. We test our model against the fused and grouped Graphical LASSO (fJGL and gJGL, respectively) of Danaher et al. (2014), the ordinary Graphical Horseshoe (GHS) of Li et al. (2019) estimated for each group independently, and the group estimation of multiple Bayesian graphical models (GemBAG) from Yang et al. (2021). Among all competing approaches, the proposed approach is the only one that provides uncertainty quantification through posterior inference on all model parameters.

Different combinations of n and p are evaluated, and the results are reported in Tables 1-4, where p_0 refers to the mean number of true significant edges across groups. Edge selection is assessed based on accuracy, the Matthews correlation coefficient (MCC), true and false positive rate (TPR and FPR, respectively) and the AUC criterion. We take the mean Frobenius loss among groups matrices to evaluate the goodness of the precision matrices estimates. Subscripts MPM and t_α indicate whether the posterior edge selection is performed based on the MPM method or with the cut-model proposed in Section 5, respectively. Hyperparameters a and b of the Beta prior on t_α should reflect prior beliefs in graphs' sparsity; to control the number of false positives, we set $a = 30$ and $b = 25$. For the fused and grouped Graphical LASSO, regulation parameters λ_1 and λ_2 are selected by performing a grid search to find the combination of values that minimizes the AIC (Danaher et al., 2014; Peterson et al., 2020). For GemBAG, hyperparameters related to the two levels of sparseness are set to $p_1 = 0.4$ and $p_2 = 0.8$ for all the considered cases. Prior variances v_0 and v_1 are estimated by minimizing the BIC criterion over a grid of values, as done in Yang et al. (2021).

In all scenarios, see tables 1-4, mGHS performs better than GHS applied to each group separately when the groups are actually similar, as it provides better selection performances in all the coupled, P2020 and full-dependence settings. Moreover, our model is the only competitor able to approach the performances of the GHS in the independent set-up. Indeed, in this case the latter shows better performances than all the other competitors for all the considered values of n and p , whereas the Graphical LASSO and GemBAG behave poorly and their selection results worsen as p increases.

The P2020 set-up provides the most realistic scheme, where the groups have similar but different precision matrices. Under these circumstances, the best model is GemBAG, which gives higher values of MCC and AUC for $p \geq 100$. The only competitive model is mGHS, which has the highest AUC when $p = 50$ and it is the only competitor able to approach GemBAG’s performances in the other considered cases.

In this simulation study, edge selection based on the cut model completely overtakes the selection procedure based on the MPM model. Indeed, the approach based on cuts strongly reduces the number of false discoveries, resulting in a higher value of the MCC index. Note that the value of the estimated threshold is affected by the choice of the prior distribution of t^α . We used $t^\alpha \sim \mathbf{Beta}(30, 25)$ across all simulation scenarios and data analyses; in our experience, this is a viable option that leads to control of the FPR even though different choices may lead to a different level of sparsity in the estimated graphs.

Finally, the GemBAG and fJGL provide the lowest values of the Frobenius loss. Except for the independent setting, none of the other methods gives better performances in terms of precision matrices estimation. GemBAG is the most efficient method, as it takes an average of only a few hours for the estimation of a network with $p = 500$. On the contrary, the mGHS provides a fully Bayesian inference at the cost of a 10-fold increase in computational time. GHS and Graphical LASSO have not been included in this case, as the computational time increases dramatically.

$n = 50, p = 50$	<i>Independent ($p_0 = 82.5$)</i>						<i>Coupled ($p_0 = 77.5$)</i>					
	Acc	MCC	TPR	FPR	AUC	Fr Loss	Acc	MCC	TPR	FPR	AUC	Fr Loss
mGHS _{MPM}	0.775 (0.018)	0.299 (0.030)	0.744 (0.040)	0.223 (0.019)	0.824 (0.027)	10.231 (1.224)	0.715 (0.039)	0.230 (0.039)	0.723 (0.048)	0.286 (0.041)	0.789 (0.037)	8.624 (1.029)
mGHS _{t_{ca}}	0.926 (0.008)	0.459 (0.038)	0.544 (0.052)	0.046 (0.009)	0.824 (0.027)	10.231 (1.224)	0.930 (0.009)	0.392 (0.055)	0.421 (0.086)	0.035 (0.012)	0.789 (0.037)	8.624 (1.209)
GHS _{MPM}	0.786 (0.015)	0.315 (0.029)	0.754 (0.037)	0.211 (0.015)	0.840 (0.024)	10.199 (1.246)	0.702 (0.047)	0.204 (0.044)	0.684 (0.048)	0.297 (0.049)	0.760 (0.040)	8.745 (0.940)
fJGL	0.873 (0.024)	0.384 (0.037)	0.648 (0.063)	0.110 (0.029)	0.769 (0.024)	9.186 (0.709)	0.907 (0.021)	0.333 (0.044)	0.437 (0.088)	0.061 (0.026)	0.688 (0.034)	7.863 (0.535)
gJGL	0.874 (0.024)	0.383 (0.036)	0.645 (0.062)	0.109 (0.028)	0.768 (0.024)	9.232 (0.720)	0.906 (0.021)	0.328 (0.043)	0.436 (0.091)	0.062 (0.027)	0.687 (0.036)	7.998 (0.557)
GemBAG _{MPM}	0.940 (0.002)	0.311 (0.052)	0.124 (0.041)	0.001 (0.002)	0.791 (0.057)	11.835 (1.150)	0.940 (0.002)	0.238 (0.064)	0.081 (0.036)	0.001 (0.002)	0.786 (0.050)	8.580 (0.775)
	<i>P2020 ($p_0 = 82.5$)</i>						<i>Full dependence ($p_0 = 85$)</i>					
	Acc	MCC	TPR	FPR	AUC	Fr Loss	Acc	MCC	TPR	FPR	AUC	Fr Loss
mGHS _{MPM}	0.796 (0.011)	0.358 (0.021)	0.822 (0.030)	0.206 (0.011)	0.875 (0.020)	8.498 (1.323)	0.716 (0.034)	0.247 (0.036)	0.735 (0.046)	0.285 (0.036)	0.792 (0.032)	8.349 (1.184)
mGHS _{t_{ca}}	0.925 (0.008)	0.532 (0.034)	0.698 (0.037)	0.059 (0.009)	0.875 (0.020)	8.498 (1.323)	0.923 (0.009)	0.408 (0.046)	0.446 (0.074)	0.041 (0.012)	0.792 (0.032)	8.349 (1.184)
GHS _{MPM}	0.795 (0.013)	0.321 (0.027)	0.748 (0.037)	0.202 (0.013)	0.840 (0.022)	9.371 (1.216)	0.670 (0.055)	0.165 (0.046)	0.631 (0.046)	0.327 (0.059)	0.710 (0.043)	8.616 (0.954)
fJGL	0.874 (0.023)	0.412 (0.046)	0.697 (0.050)	0.113 (0.025)	0.792 (0.025)	8.205 (0.702)	0.905 (0.021)	0.309 (0.056)	0.373 (0.100)	0.055 (0.028)	0.659 (0.040)	7.711 (0.611)
gJGL	0.864 (0.025)	0.376 (0.036)	0.660 (0.054)	0.121 (0.029)	0.770 (0.022)	8.851 (0.714)	0.902 (0.023)	0.293 (0.048)	0.358 (0.100)	0.057 (0.030)	0.650 (0.039)	7.989 (0.579)
GemBAG _{MPM}	0.956 (0.004)	0.580 (0.049)	0.367 (0.065)	0.001 (0.001)	0.871 (0.035)	7.835 (1.043)	0.938 (0.002)	0.318 (0.049)	0.112 (0.032)	0.000 (0.000)	0.838 (0.031)	7.984 (0.651)

Table 1: Simulation results for $n = 50$ and $p = 50$ (50 replicates). Methods mGHS and GHS are evaluated over $B = 10000$ post burn-in samples.

$n = 50, p = 100$	<i>Independent ($p_0 = 195$)</i>						<i>Coupled ($p_0 = 177.5$)</i>					
	Acc	MCC	TPR	FPR	AUC	Fr Loss	Acc	MCC	TPR	FPR	AUC	Fr Loss
mGHS _{MPM}	0.655 (0.024)	0.146 (0.018)	0.712 (0.030)	0.348 (0.025)	0.759 (0.023)	20.607 (1.444)	0.568 (0.028)	0.082 (0.020)	0.653 (0.036)	0.436 (0.028)	0.671 (0.037)	17.547 (1.283)
mGHS _{t_α}	0.953 (0.004)	0.348 (0.032)	0.361 (0.044)	0.022 (0.005)	0.759 (0.023)	20.607 (1.444)	0.961 (0.003)	0.228 (0.050)	0.152 (0.060)	0.009 (0.005)	0.671 (0.037)	17.547 (1.283)
GHS _{MPM}	0.669 (0.023)	0.155 (0.019)	0.715 (0.030)	0.333 (0.024)	0.769 (0.024)	20.594 (1.453)	0.563 (0.029)	0.074 (0.020)	0.638 (0.036)	0.439 (0.029)	0.655 (0.036)	17.545 (1.283)
fJGL	0.931 (0.012)	0.315 (0.028)	0.451 (0.054)	0.049 (0.014)	0.701 (0.022)	19.892 (0.988)	0.952 (0.009)	0.234 (0.033)	0.226 (0.074)	0.021 (0.012)	0.603 (0.032)	16.296 (0.694)
gJGL	0.929 (0.013)	0.312 (0.029)	0.456 (0.058)	0.051 (0.015)	0.702 (0.023)	19.921 (1.055)	0.952 (0.009)	0.229 (0.034)	0.219 (0.074)	0.021 (0.011)	0.599 (0.032)	16.689 (0.722)
GemBAG _{MPM}	0.962 (0.001)	0.179 (0.043)	0.052 (0.026)	0.001 (0.001)	0.698 (0.069)	23.012 (2.174)	0.965 (0.001)	0.143 (0.046)	0.034 (0.016)	0.001 (0.000)	0.708 (0.044)	16.986 (0.894)
	<i>P2020 ($p_0 = 182.5$)</i>						<i>Full dependence ($p_0 = 185$)</i>					
	Acc	MCC	TPR	FPR	AUC	Fr Loss	Acc	MCC	TPR	FPR	AUC	Fr Loss
mGHS _{MPM}	0.720 (0.013)	0.215 (0.014)	0.808 (0.025)	0.284 (0.013)	0.853 (0.016)	18.878 (1.944)	0.589 (0.030)	0.107 (0.021)	0.692 (0.036)	0.415 (0.031)	0.714 (0.035)	17.127 (1.491)
mGHS _{t_α}	0.948 (0.004)	0.459 (0.022)	0.625 (0.030)	0.040 (0.005)	0.853 (0.016)	18.878 (1.944)	0.958 (0.004)	0.285 (0.046)	0.230 (0.071)	0.013 (0.006)	0.714 (0.035)	17.127 (1.491)
GHS _{MPM}	0.710 (0.016)	0.181 (0.015)	0.733 (0.026)	0.291 (0.017)	0.800 (0.016)	20.299 (1.650)	0.564 (0.029)	0.072 (0.022)	0.626 (0.040)	0.438 (0.029)	0.647 (0.039)	17.256 (1.261)
fJGL	0.935 (0.010)	0.393 (0.030)	0.588 (0.042)	0.052 (0.011)	0.768 (0.018)	18.557 (1.070)	0.955 (0.007)	0.240 (0.042)	0.201 (0.079)	0.016 (0.010)	0.593 (0.035)	16.103 (1.027)
gJGL	0.923 (0.011)	0.335 (0.024)	0.540 (0.043)	0.062 (0.013)	0.739 (0.018)	20.104 (1.107)	0.955 (0.008)	0.223 (0.038)	0.182 (0.071)	0.015 (0.010)	0.583 (0.031)	16.772 (0.924)
GemBAG _{MPM}	0.975 (0.002)	0.550 (0.041)	0.321 (0.052)	0.000 (0.000)	0.869 (0.015)	15.676 (1.264)	0.966 (0.001)	0.277 (0.038)	0.084 (0.022)	0.000 (0.000)	0.808 (0.037)	16.411 (1.044)

Table 2: Simulation results for $n = 50$ and $p = 100$ (50 replicates). Methods mGHS and GHS are evaluated over $B = 10000$ post burn-in samples.

$n = 100, p = 250$	<i>Independent ($p_0 = 532.5$)</i>						<i>Coupled ($p_0 = 477.5$)</i>					
	Acc	MCC	TPR	FPR	AUC	Fr Loss	Acc	MCC	TPR	FPR	AUC	Fr Loss
mGHS _{M_{MPM}}	0.632 (0.012)	0.115 (0.006)	0.808 (0.015)	0.371 (0.012)	0.830 (0.012)	34.766 (1.629)	0.556 (0.010)	0.077 (0.007)	0.761 (0.021)	0.447 (0.010)	0.761 (0.018)	31.934 (1.062)
mGHS _{t_α}	0.976 (0.002)	0.420 (0.016)	0.524 (0.021)	0.015 (0.002)	0.830 (0.012)	34.766 (1.629)	0.983 (0.001)	0.350 (0.019)	0.308 (0.036)	0.007 (0.002)	0.761 (0.018)	31.934 (1.062)
GHS _{M_{MPM}}	0.639 (0.007)	0.118 (0.005)	0.812 (0.015)	0.364 (0.007)	0.835 (0.011)	34.721 (1.596)	0.551 (0.010)	0.069 (0.007)	0.729 (0.023)	0.451 (0.010)	0.732 (0.019)	32.946 (1.024)
fJGL	0.956 (0.005)	0.345 (0.016)	0.617 (0.025)	0.038 (0.006)	0.790 (0.011)	37.527 (1.235)	0.971 (0.004)	0.307 (0.020)	0.423 (0.030)	0.021 (0.004)	0.701 (0.014)	31.616 (0.839)
gJGL	0.956 (0.005)	0.344 (0.016)	0.618 (0.024)	0.038 (0.006)	0.790 (0.010)	37.581 (1.169)	0.970 (0.005)	0.292 (0.017)	0.407 (0.040)	0.022 (0.005)	0.693 (0.018)	32.616 (0.917)
GemBAG _{M_{MPM}}	0.985 (0.000)	0.344 (0.018)	0.147 (0.013)	0.000 (0.000)	0.697 (0.020)	46.156 (1.840)	0.986 (0.000)	0.326 (0.022)	0.130 (0.014)	0.000 (0.000)	0.836 (0.010)	30.824 (0.927)
	<i>P2020 ($p_0 = 482.5$)</i>						<i>Full dependence ($p_0 = 485$)</i>					
	Acc	MCC	TPR	FPR	AUC	Fr Loss	Acc	MCC	TPR	FPR	AUC	Fr Loss
mGHS _{M_{MPM}}	0.654 (0.007)	0.132 (0.004)	0.863 (0.013)	0.350 (0.007)	0.885 (0.008)	26.270 (1.321)	0.575 (0.011)	0.095 (0.006)	0.811 (0.017)	0.429 (0.011)	0.815 (0.014)	30.133 (1.058)
mGHS _{t_α}	0.972 (0.002)	0.460 (0.013)	0.699 (0.017)	0.024 (0.002)	0.885 (0.008)	26.270 (1.321)	0.981 (0.002)	0.406 (0.017)	0.440 (0.034)	0.011 (0.002)	0.815 (0.014)	30.133 (1.058)
GHS _{M_{MPM}}	0.659 (0.007)	0.123 (0.005)	0.817 (0.015)	0.344 (0.007)	0.850 (0.010)	29.366 (1.298)	0.552 (0.010)	0.068 (0.007)	0.725 (0.022)	0.451 (0.010)	0.728 (0.018)	32.782 (0.948)
fJGL	0.963 (0.004)	0.416 (0.018)	0.717 (0.021)	0.033 (0.004)	0.842 (0.009)	31.347 (1.244)	0.972 (0.004)	0.395 (0.022)	0.559 (0.040)	0.021 (0.004)	0.769 (0.019)	26.937 (1.079)
gJGL	0.954 (0.006)	0.347 (0.020)	0.655 (0.023)	0.041 (0.006)	0.807 (0.010)	37.849 (1.392)	0.969 (0.005)	0.291 (0.017)	0.413 (0.042)	0.023 (0.006)	0.695 (0.019)	32.168 (0.913)
GemBAG _{M_{MPM}}	0.992 (0.000)	0.713 (0.010)	0.516 (0.013)	0.000 (0.000)	0.893 (0.007)	18.421 (0.865)	0.989 (0.000)	0.534 (0.017)	0.293 (0.017)	0.000 (0.000)	0.893 (0.008)	26.442 (0.976)

Table 3: Simulation results for $n = 100$ and $p = 250$ (50 replicates). Methods mGHS and GHS are evaluated over $B = 10000$ post burn-in samples.

$n = 100, p = 500$	<i>Independent</i> ($p_0 = 271.25$)						<i>Coupled</i> ($p_0 = 279.5$)					
	Acc	MCC	TPR	FPR	AUC	Fr Loss	Acc	MCC	TPR	FPR	AUC	Fr Loss
mGHS _{MPM}	0.518 (0.003)	0.034 (0.002)	0.845 (0.023)	0.482 (0.003)	0.832 (0.018)	41.906 (1.633)	0.525 (0.004)	0.043 (0.002)	0.929 (0.014)	0.476 (0.004)	0.922 (0.010)	39.677 (1.851)
mGHS _{t_α}	0.997 (0.000)	0.430 (0.021)	0.461 (0.030)	0.001 (0.000)	0.832 (0.018)	41.906 (1.633)	0.994 (0.003)	0.425 (0.064)	0.747 (0.022)	0.006 (0.003)	0.922 (0.010)	39.677 (1.851)
GemBAG _{MPM}	0.998 (0.000)	0.379 (0.032)	0.172 (0.023)	0.000 (0.000)	0.799 (0.013)	40.747 (1.495)	0.999 (0.000)	0.740 (0.015)	0.634 (0.036)	0.000 (0.000)	0.962 (0.014)	33.100 (3.257)
	<i>P2020</i> ($p_0 = 270.5$)						<i>Full Dependence</i> ($p_0 = 273$)					
	Acc	MCC	TPR	FPR	AUC	Fr Loss	Acc	MCC	TPR	FPR	AUC	Fr Loss
mGHS _{MPM}	0.522 (0.004)	0.041 (0.002)	0.915 (0.018)	0.479 (0.003)	0.909 (0.015)	38.121 (2.107)	0.523 (0.004)	0.043 (0.002)	0.938 (0.016)	0.478 (0.004)	0.933 (0.013)	38.741 (2.042)
mGHS _{t_α}	0.979 (0.013)	0.274 (0.085)	0.770 (0.020)	0.020 (0.013)	0.909 (0.015)	38.121 (2.107)	0.979 (0.013)	0.286 (0.080)	0.819 (0.019)	0.020 (0.013)	0.933 (0.013)	38.741 (2.042)
GemBAG _{MPM}	0.999 (0.000)	0.839 (0.012)	0.723 (0.030)	0.000 (0.000)	0.966 (0.011)	23.992 (4.506)	0.999 (0.000)	0.873 (0.014)	0.771 (0.028)	0.000 (0.000)	0.979 (0.006)	22.112 (3.407)

Table 4: Simulation results for $n = 100$ and $p = 500$ (25 replicates). Method mGHS is evaluated over $B = 10000$ post burn-in samples.

7 Application to a bike-sharing dataset

We perform an analysis of the Capital Bikeshare system data¹, a benchmark dataset previously analyzed in Zhu and Foygel Barber (2015) and Yang et al. (2021). This is the first analysis of this dataset with a full Bayesian graphical model. The dataset contains records of bike rentals in a bicycle sharing system with more than 500 stations located in the Washington D.C. area, where each ride is labeled as *casual* (paying for a single day) or *member* (membership payment). Data from years 2016, 2017, and 2018 are used, for a total of $n = 1092$ registered days. Only the $p = 239$ most active stations are selected. Therefore, for $i = 1, \dots, 1092$ and $j = 1, \dots, 239$, let y_{ij}^c and y_{ij}^m be the number of registered casual and member trips initiated at station j on day i , respectively. After correcting for the seasonal trend, each station data is marginally standardized and transformed with the Yeo-Johnson transformation (Yeo and Johnson, 2000) to better approximate a Gaussian distribution. Finally, the data are divided by year and rider membership for a total of $K = 6$ groups. Matrices \mathbf{Y}_k , $k = 1, \dots, 6$ are marginally standardized such that $\boldsymbol{\mu}_k = \mathbf{0}$

¹Data are available at <http://www.capitalbikeshare.com/system-data>

and the standard deviations are equal to 1 for each group.

For each class, 80% of the observations are used as training set and the remaining 20% as test set. For $k = 1, \dots, 6$, let $\hat{\Omega}_k$ be the estimated precision matrix of the k -th training set. Here we take the posterior mean. Following Fan et al. (2009), the observations of each test set is partitioned as $\mathbf{y}_i^k = (\mathbf{y}_{i,j_1}^k, \mathbf{y}_{i,j_2}^k)$, where $\mathbf{y}_{i,j_1}^k = (y_{i,1}^k, \dots, y_{i,120}^k)$ and $\mathbf{y}_{i,j_2}^k = (y_{i,121}^k, \dots, y_{i,239}^k)$, $i = 1, \dots, n_k$. The corresponding partition for Ω_k and Σ_k are

$$\Omega_k = \begin{bmatrix} \Omega_{k11} & \Omega_{k12} \\ \Omega_{k21} & \Omega_{k22} \end{bmatrix} \quad \text{and} \quad \Sigma_k = \begin{bmatrix} \Sigma_{k11} & \Sigma_{k12} \\ \Sigma_{k21} & \Sigma_{k22} \end{bmatrix}.$$

The performances of the models are evaluated by predicting \mathbf{y}_{i,j_2}^k based on \mathbf{y}_{i,j_1}^k and $\hat{\Omega}_k$. Under the Gaussian assumption, the best linear predictor is

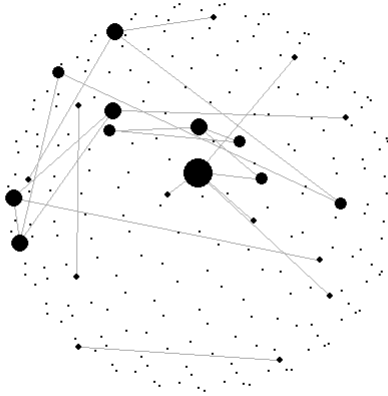
$$\hat{\mathbf{y}}_{i,j_2}^k = \mathbb{E}(\mathbf{y}_{i,j_2}^k \mid \mathbf{y}_{i,j_1}^k) = \hat{\Sigma}_{k21} \hat{\Sigma}_{k11}^{-1} \mathbf{y}_{i,j_1}^k.$$

To assess the prediction performances of the methods we rely on the *average absolute forecast error* (AAFE), defined as

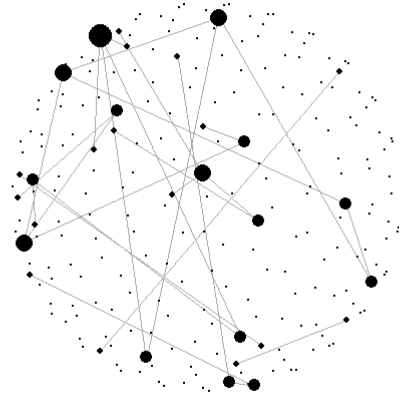
$$\text{AAFE}_k = \frac{1}{119} \frac{1}{|\mathbb{T}_k|} \sum_{i \in \mathbb{T}_k} \sum_{j=121}^{239} |y_{ij}^k - \hat{y}_{ij}^k|,$$

where \mathbb{T}_k denotes the test set indexes for group k . We denote the mean AAFE across groups as mAAFE.

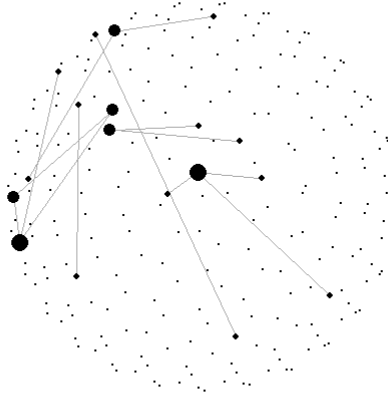
The multiple Graphical Horseshoe is tested against the ordinary Graphical Horseshoe of Li et al. (2019) and the GemBAG of Yang et al. (2021). For the estimation of the threshold in the mGHS model we set the hyperparameter to $a = 30$ and $b = 25$, whereas in GemBAG we estimated hyperparameters v_0 and v_1 according to the BIC criterion as in Section 6. For computational reasons, the joint Graphical LASSO of Danaher et al. (2014) is excluded from the analysis. We checked the convergence of mGHS algorithm by estimating the potential scale reduction factor (psrf, Gelman and Rubin, 1992) of parameters ω_{ij}^K , $i = 1, \dots, 239$, $j > i$, $k = 1, \dots, 6$, over 4 replications. The distribution of the estimated psrf is shown in Figure 1 of the Supplementary Material; roughly 99% of the estimated values lie in the interval $[1.0, 1.2]$. Finally, the trace plots of the log-posterior are shown in Figure 2 of the Supplementary Material and do not suggest a lack of convergence of the chains.



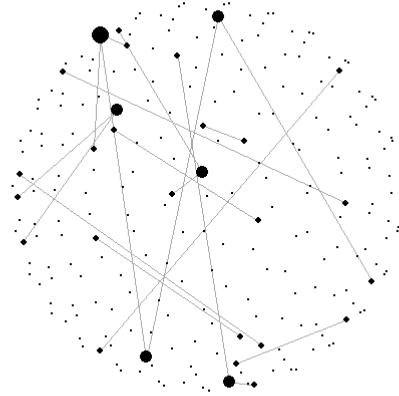
(a) Casual network estimated by mGHS



(b) Member network estimated by mGHS



(c) Casual network estimated by GHS



(d) Member network estimated by GHS

Figure 3: Intersection of the estimated networks across three years; the size of the nodes depends on the number of edges associated to the related station

With $mAAFE = 0.596$, the best predictive model is the mGHS, whereas the ordinary GHS shows similar predictive performance ($mAAFE = 0.600$). The latter, however, provides a sparser model: regardless of the method used for selecting the edges a posteriori, the mGHS always

estimates denser networks, including connections between stations that the GHS is not able to capture. Finally, the GemBAG provides at the same time the sparsest model and the worst predictive performance, with $mAAFE = 0.613$.

To further understand how the connections between stations work among the casual and member users, we plot the estimated networks for each group for both GHS and mGHS (Figures 3 and 4 in Appendix B of Supplementary Materials), where we select those edges with a posterior inclusion probability higher than 0.9. The estimated networks for casual users are denser in both models, suggesting a higher activity of casual rides. However, the number of edges shared across the years is higher for the registered users, implying more regular activities of those who choose to pay a seasonal ticket. The intersection of the estimated networks across three years for the registered and casual users is shown in Figure 3 for both GHS and mGHS, where the size of the nodes depends on the number of edges associated with the related stations. The two models estimate similar networks for both types of users, however, mGHS gives more importance to the stations identified by GHS and includes some additional ones.

The hypothesis of a more regular behavior of the registered users is supported also by the estimated correlation matrix between groups, i.e. the posterior mean of \mathbf{R} :

$$\hat{\mathbf{R}} = \begin{pmatrix} \text{casual 2016} & \text{casual 2017} & \text{casual 2018} & \text{member 2016} & \text{member 2017} & \text{member 2018} \\ \left(\begin{array}{cccccc} 1.000 & 0.969 & 0.893 & 0.479 & 0.515 & 0.483 \\ 0.969 & 1.000 & 0.958 & 0.518 & 0.562 & 0.526 \\ 0.893 & 0.958 & 1.000 & 0.461 & 0.502 & 0.475 \\ 0.479 & 0.518 & 0.461 & 1.000 & 0.984 & 0.971 \\ 0.515 & 0.562 & 0.502 & 0.984 & 1.000 & 0.980 \\ 0.483 & 0.526 & 0.475 & 0.971 & 0.980 & 1.000 \end{array} \right) & \begin{array}{l} \text{casual 2016} \\ \text{casual 2017} \\ \text{casual 2018} \\ \text{member 2016} \\ \text{member 2017} \\ \text{member 2018} \end{array} \end{pmatrix}$$

The correlation is high across the years for both types of users. In particular, it remains close to 1 even after two years for the rides with membership payment (correlation between 2016 and 2018 is 0.971). On the contrary, the decrease is larger for the casual rides, with a correlation of 0.893.

8 Conclusion

We have introduced a novel fully Bayesian method for the analysis of high-dimensional dependent precision matrices. In particular, we provided an efficient approach that works up to hundreds of variables. We empirically showed that the model is able to borrow information between groups

when appropriately supported by the data. Simulation studies empirically demonstrated that the proposed approach has good performances in terms of edge selection; the proposed joint model performs at least as well as the separate analysis of each group with the ordinary Graphical Horseshoe (Li et al., 2019). We applied our method to a benchmark dataset with a slight improvement in prediction performance. Compared to the ordinary Graphical Horseshoe, the proposed model borrowed information across groups and selected a higher number of common edges across the years. Moreover, the estimation of correlation matrix \mathbf{R} provided unique insights about the behavior of bike-sharing users. We also proposed a new approach for posterior edge selection that accounts for posterior dependencies between parameters $\lambda_{ij,k}^2$'s. This method can be easily extended to other common frameworks, for example, variable selection in regression models. Further improvements concern the introduction of different thresholds t_{ij}^α behavior edge or adaptive methods to improve the proposal distribution. The proposed cut model provides only an approximation of the posterior distribution, and, in models with cuts in general, the algorithm may fail to converge to a well-defined distribution (Plummer, 2015). Whereas cut models can outperform fully Bayesian models in terms of performance and computational efficiency, a careful assessment of the output produced by models with cuts should be always performed.

Note that very recently Lingjaerde et al. (2022) have proposed an approach, alternative to the one presented in this paper, for the analysis of multiple graphical models with horseshoe priors, termed the joint graphical horseshoe. The approach proposed in this paper, with respect to the joint graphical horseshoe, is characterized by a few important and unique features, since it provides full Bayesian inference, it adapts well to setting with heterogeneous levels of network similarity, it learns the level of network similarity across groups from the data, and it has been successfully applied to networks with large p (up to 500 nodes).

Among possible extensions, we may consider a spike-and-slab type of prior on the off-diagonal elements of the correlation matrix \mathbf{R} . This approach would not only give a deeper insight into the similarity across the groups, but it would speed the model up when the groups are not significantly related: the \mathcal{G}_{3p} distribution would reduce to an Inverse-Gamma when the k -th row of the matrix \mathbf{R} is zero, avoiding the need of the rejection sampling discussed in Section 3.

A main challenge, and still a limitation, of the proposed approach, is the computational complexity of the algorithm since it becomes infeasible when the number of covariates p is extremely

large, e.g., in the thousands. Alternative computational approaches that could be explored include the thresholding approach of Johndrow et al. (2020) that could be adapted to sample from multivariate Normal distributions under the Horseshoe prior, and eventually lead to a significant reduction in computational times.

The R code for mGHS model, simulations studies and application to bike-sharing dataset is available at <https://github.com/cbusatto/mGHS>.

Supplementary Materials

In Supplementary Materials (file `mGHS_suppl_mat.pdf`) can be found:

mGHS algorithm: the pseudo-code for mGHS algorithm can be found in Appendix A.

Supplementary Figures: distribution of the estimated psrf and post-burnin trace of the log-posterior distribution of the 4 chains for the analysis of the convergence of mGHS algorithm are shown in Figure 1 and 2 of Appendix B, respectively, whereas estimated networks by both GHS and mGHS models for bike-sharing dataset are given in Figures 3 and 4 of Appendix B.

Acknowledgments

Funding details

Both authors were partially supported by the “Dipartimenti Eccellenti 2018-2022” ministerial funds (Italy).

Disclosure statement

The authors report there are no competing interests to declare.

References

- Ahrens, J. H. and Dieter, U. (1982). Generating Gamma variates by a modified rejection technique. Commun. ACM, 25(1):47–54.
- Barbieri, M. M. and Berger, J. O. (2004). Optimal predictive model selection. The Annals of Statistics, 32(3):870–897.
- Barbieri, M. M., Berger, J. O., George, E. I., and Ročková, V. (2021). The Median Probability Model and correlated variables. Bayesian Analysis, 16(4):1085–1112.
- Barnard, J., McCulloch, R., and Meng, X.-L. (2000). Modeling covariance matrices in terms of standard deviations and correlations, with application to shrinkage. Statistica Sinica, 10(4):1281–1311.
- Bayarri, M. J., Berger, J. O., and Liu, F. (2009). Modularization in Bayesian analysis, with emphasis on analysis of computer models. Bayesian Analysis, 4(1):119–150.
- Bhadra, A., Datta, J., Li, Y., Polson, N., and Willard, B. (2016). Prediction risk for global-local shrinkage regression.
- Blangiardo, M., Hansell, A., and Richardson, S. (2011). A Bayesian model of time activity data to investigate health effect of air pollution in time series studies. Atmospheric Environment-ATMOS ENVIRON, 45:379–386.
- Carvalho, C. M., Polson, N. G., and Scott, J. G. (2010). The horseshoe estimator for sparse signals. Biometrika, 97:465–480.
- Danaher, P. J., Wang, P., and Witten, D. M. (2014). The joint Graphical LASSO for inverse covariance estimation across multiple classes. Journal of the Royal Statistical Society. Series B, Statistical methodology, 76(2):373–397.
- Dempster, A. P. (1972). Covariance selection. Biometrics, 28(1):157–175.
- Dieter, U. (1981). Optimal acceptance-rejection envelopes for sampling from various distributions. Mathematics of Computation.

- Fan, J., Feng, Y., and Wu, Y. (2009). Network exploration via the adaptive LASSO and SCAD penalties. The Annals of Applied Statistics, 3(2):521–541.
- Friedman, J., Hastie, T., and Tibshirani, R. (2008). Sparse inverse covariance estimation with the Graphical LASSO. Biostatistics, 9(3):432–441.
- Gelman, A. and Rubin, D. B. (1992). Inference from iterative simulation using multiple sequences. Statistical Science, 7(4):457–472.
- Johndrow, J. E., Orenstein, P., and Bhattacharya, A. (2020). Scalable approximate MCMC algorithms for the Horseshoe prior. Journal of Machine Learning Research, 21:73:1–73:61.
- Li, Y., Craig, B. A., and Bhadra, A. (2019). The Graphical Horseshoe estimator for inverse covariance matrices. Journal of Computational and Graphical Statistics, 28(3):747–757.
- Lingjaerde, C., Fairfax, B. P., Richardson, S., and Ruffieux, H. (2022). Scalable multiple network inference with the joint graphical horseshoe. arXiv:2206.11820.
- Liu, X. and Daniels, M. J. (2006). A new algorithm for simulating a correlation matrix based on parameter expansion and reparameterization. Journal of Computational and Graphical Statistics, 15:897–914.
- Lunn, D., Best, N., Spiegelhalter, D., Graham, G., and Neuenschwander, B. (2009). Combining MCMC with ‘sequential’ PKPD modelling. Journal of pharmacokinetics and pharmacodynamics, 36:19–38.
- Makalic, E. and Schmidt, D. F. (2016). A simple sampler for the Horseshoe estimator. IEEE Signal Processing Letters, 23(1):179–182.
- McCandless, L. C., Douglas, I. J., Evans, S. J., and Smeeth, L. (2010). Cutting feedback in Bayesian regression adjustment for the Propensity Score. The International Journal of Biostatistics, 6(2).
- Ni, Y., Baladandayuthapani, V., Vannucci, M., and Stingo, F. (2022). Bayesian graphical models for modern biological applications (with discussion). Statistical Methods and Applications, 31:197–225.

- Peterson, C., Stingo, F., and Vannucci, M. (2015). Bayesian inference of multiple Gaussian graphical models. Journal of the American Statistical Association, 110(509):159–174.
- Peterson, C. B., Osborne, N., Stingo, F. C., Bourgeat, P., Doecke, J. D., and Vannucci, M. (2020). Bayesian modeling of multiple structural connectivity networks during the progression of Alzheimer’s disease. Biometrics, 76(4):1120–1132.
- Plummer, M. (2015). Cuts in Bayesian graphical models. Statistics and Computing, page 37–43.
- Pourahmadi, M. (2011). Covariance estimation: The GLM and regularization perspectives. Statistical Science, 26(3):369–387.
- Segura, J. (2021). Uniform (very) sharp bounds for ratios of Parabolic Cylinder functions. Studies in Applied Mathematics, 147.
- Shaddox, E., Stingo, F., Peterson, C., Jacobson, S., Cruickshank-Quinn, C., Kechris, K., Bowler, R., and Vannucci, M. (2018). A Bayesian approach for learning gene networks underlying disease severity in COPD. Statistics in Biosciences, 10(1):59–85.
- Stadlober, E. (1982). Generating Student’s T Variates by a Modified Rejection Method, pages 349–360. Springer Netherlands.
- Van der Pas, S., Kleijn, B. J., and van der Vaart, A. (2014). The Horseshoe estimator: Posterior concentration around nearly black vectors. Electronic Journal of Statistics, 8.
- Van der Pas, S., Szabó, B., and van der Vaart, A. (2017). Uncertainty quantification for the Horseshoe (with discussion). Bayesian Analysis, 12(4):1221–1274.
- Wang, H. (2012). Bayesian Graphical Lasso models and efficient posterior computation. Bayesian Analysis, 7.
- Wang, H. (2015). Scaling it up: Stochastic search structure learning in graphical models. Bayesian Analysis, 10(2):351–377.
- Yang, X., Gan, L., Narisetty, N., and Liang, F. (2021). Gembag: Group estimation of multiple Bayesian graphical models. Journal of Machine Learning Research, 22.

- Yeo, I.-K. and Johnson, R. A. (2000). A new family of power transformations to improve normality or symmetry. Biometrika, 87(4):954–959.
- Zhu, Y. and Foygel Barber, R. (2015). The log-shift penalty for adaptive estimation of multiple gaussian graphical models. In Proceedings of the Eighteenth International Conference on Artificial Intelligence and Statistics, pages 1153–1161.
- Zigler, C. (2016). The central role of Bayes theorem for joint estimation of causal effects and Propensity Scores. The American Statistician, 70:47–54.
- Zigler, C., Watts, K., Yeh, R., Wang, Y., Coull, B., and Dominici, F. (2013). Model feedback in Bayesian Propensity Score estimation. Biometrics, 69.

A Appendix A

A.1 Technical details of the modified rejection sampling method

The acceptance probability of each step of the algorithm is compute as follows:

- Step 1: the probability of immediate acceptance is

$$P(E_1) = \Phi_{0,\omega^2}(t_2) - \Phi_{0,\omega^2}(t_1),$$

where $\Phi_{\mu,\sigma^2}(\cdot)$ denotes the cumulative density function of a gaussian distribution with mean μ and variance σ^2 ;

- Step 2: the acceptance probability of Step 2 is

$$P(E_2) = 1 - P(E_1) - P(E_3),$$

where $P(E_3)$ is the acceptance probability of Step 3.

- Step 3: the probability of acceptance this step is

$$\begin{aligned} P(E_3) &= \int_{-\infty}^{t_1} h(t)dt + \int_{t_2}^{\infty} h(t)dt - \int_{-\frac{\mu}{\sigma}}^{t_1} g(t)dt + \int_{t_2}^{\infty} g(t)dt \\ &= \int_{-\infty}^{\infty} h(t)dt - \int_{t_1}^{t_2} h(t)dt - \int_{-\frac{\mu}{\sigma}}^{\infty} g(t)dt + \int_{t_1}^{t_2} g(t)dt \\ &= \int_{t_1}^{t_2} g(t) - h(t)dt. \end{aligned}$$

A.2 Rejection sampling for sampling from the difference distribution

$d(t)$

Sampling from $d(t)$ in Step 3 can be achieved by means of a standard rejection sampling. Let $s(t)$ be the proposal distribution, we adapt a double-exponential (Laplace) distribution of the form

$$s(t) = \frac{c}{\sqrt{2\pi}} e^{-\frac{|t-b|}{\delta}}, \quad -\infty < t < \infty,$$

in order to minimize the area between $s(t)$ and $d(t)$ (Ahrens and Dieter, 1982; Stadlober, 1982). This happens when the hat function $s(t)$ touches $d(t)$ at two different points L and R , with $R > L$.

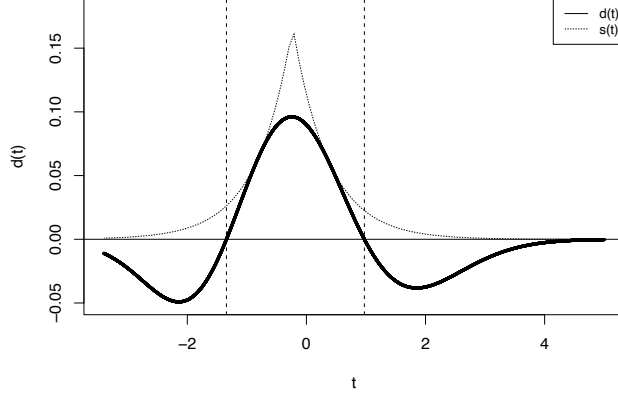


Figure 4: distributions $d(t)$ and $s(t)$; dotted lines represent t_1 and t_2 .

As explained in Dieter (1981), if $d(t)$ is covered by a double-exponential distribution, optimal parameters c , b , and δ can be estimated within two steps: first, points L , R and parameter δ are computed simultaneously (for instance by Newton iteration) as

$$\begin{aligned} d'(L) &= \frac{1}{\delta}d(L) \\ d'(R) &= -\frac{1}{\delta}d(R) \\ \delta &= \frac{1}{2}(R - L), \end{aligned}$$

whereas parameters c and b are calculated as

$$\begin{aligned} b &= \frac{1}{2} \left(L + R + \delta \ln \left(\frac{d(R)}{d(L)} \right) \right) \\ c &= e \sqrt{2\pi d(R)d(L)}. \end{aligned}$$

Figure 4 shows the difference function $d(t)$ and its optimal hat function $s(t)$.

The algorithm can be further sped up by noting that the quantities t_1 , t_2 , b , c and δ only depend on the ratio β/α . The computation of these parameters, which involve iterative methods, can be avoided by tabulating the needed quantities for a restricted grid of the parameters γ , α , and β .

A.3 Proof of Proposition 3.1

Recalling that $t = (x - \mu)/\sigma$, where $x > 0$, the acceptance probability of the first two steps of the algorithm can be computed as

$$\begin{aligned}
 \mathbb{P}(T_{acc}) &= \mathbb{P}\left(U \leq \frac{g(t)}{h(t)}\right) \\
 &= \int_{-\frac{\mu}{\sigma}}^{\infty} \mathbb{P}\left(U \leq \frac{g(t)}{h(t)} \mid T = t\right) h(t) dt \\
 &= \int_{-\frac{\mu}{\sigma}}^{t_1} \frac{g(t)}{h(t)} h(t) dt + \int_{t_1}^{t_2} h(t) dt + \int_{t_2}^{\infty} \frac{g(t)}{h(t)} h(t) dt \\
 &= \int_{-\frac{\mu}{\sigma}}^{t_1} g(t) dt + \int_{t_1}^{t_2} h(t) dt + \int_{t_2}^{\infty} g(t) dt.
 \end{aligned}$$

Thus, the probability of rejection is $\mathbb{P}(T_{rej}) = 1 - \mathbb{P}(T_{acc}) = \int_{t_1}^{t_2} g(t) - h(t) dt$. Since the Step 3 draws a sample from $\int_{t_1}^{t_2} g(t) - h(t) dt$, the acceptance probability of the method is exactly 1.

To show that the distribution of accepted values follows the target density $g(t)$, the cumulative density function $\mathbb{P}(T \leq u \mid T_{acc}) = \frac{\mathbb{P}(T \leq u, T_{acc})}{\mathbb{P}(T_{acc})} = \mathbb{P}(T \leq u, T_{acc})$ has to be equal to $F_{g(t)}(u) = \int_{-\frac{\mu}{\sigma}}^u g(t) dt$. Three different cases are studied:

- **Case $u < t_1$:**

$$\begin{aligned}
 \mathbb{P}(T \leq u, T_{acc}) &= \int_{-\frac{\mu}{\sigma}}^u \mathbb{P}\left(U \leq \frac{g(t)}{h(t)}\right) h(t) dt \\
 &= \int_{-\frac{\mu}{\sigma}}^u g(t) dt \\
 &= F_{g(t)}(u);
 \end{aligned}$$

- **Case $u \in [t_1, t_2]$:**

$$\begin{aligned}
 \mathbb{P}(T \leq u, T_{acc}) &= \mathbb{P}(T \leq t_1, T_{acc}) + \mathbb{P}(t_1 < T \leq u, T_{acc}) \\
 &= F_{g(t)}(t_1) + \int_{t_1}^u \mathbb{P}\left(U \leq \frac{g(t)}{h(t)}\right) h(t) dt + \int_{t_1}^u g(t) - h(t) dt \\
 &= F_{g(t)}(t_1) + \int_{t_1}^u h(t) dt + \int_{t_1}^u g(t) - h(t) dt \\
 &= F_{g(t)}(u);
 \end{aligned}$$

- **Case $t_2 < u$:**

$$\begin{aligned}
\mathbb{P}(T \leq u, T_{acc}) &= \mathbb{P}(T \leq t_2, T_{acc}) + \mathbb{P}(t_2 < T \leq u, T_{acc}) \\
&= F_{g(t)}(t_2) + \int_{t_2}^u \mathbb{P}\left(U \leq \frac{g(t)}{h(t)}\right) h(t) dt \\
&= F_{g(t)}(t_2) + \int_{t_2}^u g(t) dt \\
&= F_{g(t)}(u).
\end{aligned}$$

Therefore, the method actually samples from the target distribution.

B KL divergence for the \mathcal{G}_{3p} distribution

Here the asymptotic behaviour of a \mathcal{G}_{3p} distribution for limit cases $\beta/\alpha \rightarrow -\infty$, $\beta/\alpha \rightarrow \infty$ and $\gamma \rightarrow \infty$ is described. The analysis relies on the KL divergence. In the first case, $\beta/\alpha \rightarrow -\infty$ the \mathcal{G}_{3p} distribution is compared to a Gamma distribution and yields a closed-form result, whereas when $\beta/\alpha \rightarrow \infty$ and $\gamma \rightarrow \infty$ the target density is approximated with a Gaussian distribution based on empirical results.

- **Proof of Proposition 3.2:**

The KL divergence between distribution $q_x \sim \mathcal{G}_{3p}(\gamma, \alpha, \beta)$ and distribution $p_x \sim \text{Ga}(d, c)$ is

$$\text{KL}(p||q) = \int_0^\infty p_x \log\left(\frac{p_x}{q_x}\right) dx = \int_0^\infty p_x \log(p_x) dx - \int_0^\infty p_x \log(q_x) dx. \quad (14)$$

Denoting the two integrals in (14) as $I(d, c) = \int_0^\infty p_x \log(p_x) dx$ and $I(d, c, \gamma, \alpha, \beta) = \int_0^\infty p_x \log(q_x) dx$, it yields

$$\begin{aligned}
I(d, c) &= \int_0^\infty \log\left(\frac{c^d}{\Gamma(d)} e^{-cx} x^{d-1}\right) \frac{c^d}{\Gamma(d)} e^{-cx} x^{d-1} dx \\
&= \log\left(\frac{c^d}{\Gamma(d)}\right) - \frac{c^{d+1}}{\Gamma(d)} \int_0^\infty e^{-cx} x^d dx + \frac{c^d(d-1)}{\Gamma(d)} \int_0^\infty \log(x) e^{-cx} x^{d-1} dx \\
&= \log\left(\frac{c^d}{\Gamma(d)}\right) - \frac{c^{d+1}}{\Gamma(d)} \frac{\Gamma(d+1)}{c^{d+1}} + \frac{c^d(d-1)}{\Gamma(d)} \frac{\Gamma(d)}{c^d} \left(\frac{\Gamma'(d)}{\Gamma(d)} - \log c\right) \\
&= \log\left(\frac{c^d}{\Gamma(d)}\right) - d + (d-1) \left(\frac{\Gamma'(d)}{\Gamma(d)} - \log c\right) \\
&= \log(c) + (d-1) \frac{\Gamma'(d)}{\Gamma(d)} - d - \log(\Gamma(d))
\end{aligned}$$

and

$$\begin{aligned}
I(d, c, \gamma, \alpha, \beta) &= \int_0^\infty \log \left(\frac{(2\alpha^2)^{\frac{\gamma+1}{2}} e^{-\frac{\beta^2}{8\alpha^2}}}{\gamma! D_{-\gamma-1} \left(-\frac{\beta}{\alpha\sqrt{2}} \right)} e^{-\alpha^2 x^2 + \beta x} x^\gamma \right) \frac{c^d}{\Gamma(d)} e^{-cx} x^{d-1} dx \\
&= \log \left(\frac{(2\alpha^2)^{\frac{\gamma+1}{2}} e^{-\frac{\beta^2}{8\alpha^2}}}{\gamma! D_{-\gamma-1} \left(-\frac{\beta}{\alpha\sqrt{2}} \right)} \right) + \frac{c^d}{\Gamma(d)} \int_0^\infty (-\alpha^2 x^2 + \beta x) e^{-cx} x^{d-1} dx \\
&\quad + \frac{c^d \gamma}{\Gamma(d)} \int_0^\infty \log(x) e^{-cx} x^{d-1} dx \\
&= \log \left(\frac{(2\alpha^2)^{\frac{\gamma+1}{2}} e^{-\frac{\beta^2}{8\alpha^2}}}{\gamma! D_{-\gamma-1} \left(-\frac{\beta}{\alpha\sqrt{2}} \right)} \right) - \frac{\alpha^2 c^d \Gamma(d+2)}{c^{d+2} \Gamma(d)} + \frac{\beta c^d \Gamma(d+1)}{c^{d+1} \Gamma(d)} + \gamma \left(\frac{\Gamma'(d)}{\Gamma(d)} - \log(c) \right) \\
&= \log \left(\frac{(2\alpha^2)^{\frac{\gamma+1}{2}} e^{-\frac{\beta^2}{8\alpha^2}}}{\gamma! D_{-\gamma-1} \left(-\frac{\beta}{\alpha\sqrt{2}} \right)} \right) - \frac{\alpha^2 d(d+1)}{c^2} + \frac{\beta d}{c} + \gamma \left(\frac{\Gamma'(d)}{\Gamma(d)} - \log(c) \right).
\end{aligned}$$

Thus,

$$\begin{aligned}
I(d, c) - I(d, c, \gamma, \alpha, \beta) &= \log(c) + (d-1) \frac{\Gamma'(d)}{\Gamma(d)} - d - \log(\Gamma(d)) - \log \left(\frac{(2\alpha^2)^{\frac{\gamma+1}{2}} e^{-\frac{\beta^2}{8\alpha^2}}}{\gamma! D_{-\gamma-1} \left(-\frac{\beta}{\alpha\sqrt{2}} \right)} \right) \\
&\quad + \frac{\alpha^2 d(d+1)}{c^2} - \frac{\beta d}{c} - \gamma \left(\frac{\Gamma'(d)}{\Gamma(d)} - \log(c) \right) \\
&= (\gamma+1) \log(c) + (d-1-\gamma) \frac{\Gamma'(d)}{\Gamma(d)} - d \left(1 + \frac{\beta}{c} - \frac{\alpha^2(d+1)}{c^2} \right) \\
&\quad + \log \left(\frac{\Gamma(\gamma+1)}{\Gamma(d)} \right) - \log \left(\frac{(2\alpha^2)^{\frac{\gamma+1}{2}} e^{-\frac{\beta^2}{8\alpha^2}}}{D_{-\gamma-1} \left(-\frac{\beta}{\alpha\sqrt{2}} \right)} \right). \tag{15}
\end{aligned}$$

Let $d = \frac{\mu^2}{\sigma^2}$ and $c = \frac{\mu}{\sigma^2}$ so that the Gamma distribution has the same mean and variance of the \mathcal{G}_{3p} distribution. Exploiting the properties of the Parabolic Cylinder functions it yields

$$\begin{aligned}
\lim_{\frac{\beta}{\alpha} \rightarrow -\infty} d &= \lim_{\frac{\beta}{\alpha} \rightarrow -\infty} \frac{(\gamma+1)^2 D_{-\gamma-2} \left(-\frac{\beta}{\alpha\sqrt{2}}\right)^2}{D_{-\gamma-1} \left(-\frac{\beta}{\alpha\sqrt{2}}\right)} \left(\frac{\gamma+2}{\gamma+1} D_{-\gamma-3} \left(-\frac{\beta}{\alpha\sqrt{2}}\right) - \frac{D_{-\gamma-2} \left(-\frac{\beta}{\alpha\sqrt{2}}\right)^2}{D_{-\gamma-1} \left(-\frac{\beta}{\alpha\sqrt{2}}\right)} \right)^{-1} \\
&= \frac{1}{\lim_{\frac{\beta}{\alpha} \rightarrow -\infty} \frac{D_{-\gamma-1} \left(-\frac{\beta}{\alpha\sqrt{2}}\right)}{(\gamma+1) D_{-\gamma-2} \left(-\frac{\beta}{\alpha\sqrt{2}}\right)^2} \left((\gamma+2) D_{-\gamma-3} \left(-\frac{\beta}{\alpha\sqrt{2}}\right) - (\gamma+1) \frac{D_{-\gamma-2} \left(-\frac{\beta}{\alpha\sqrt{2}}\right)^2}{D_{-\gamma-1} \left(-\frac{\beta}{\alpha\sqrt{2}}\right)} \right)} \\
&= \frac{1}{\lim_{\frac{\beta}{\alpha} \rightarrow -\infty} \frac{(\gamma+2) D_{-\gamma-3} \left(-\frac{\beta}{\alpha\sqrt{2}}\right) D_{-\gamma-1} \left(-\frac{\beta}{\alpha\sqrt{2}}\right)}{(\gamma+1) D_{-\gamma-2} \left(-\frac{\beta}{\alpha\sqrt{2}}\right)^2} - 1} \\
&= \frac{1}{\frac{\gamma+2}{\gamma+1} - 1} = \gamma + 1
\end{aligned}$$

and

$$\begin{aligned}
\lim_{\frac{\beta}{\alpha} \rightarrow -\infty} c &= \lim_{\frac{\beta}{\alpha} \rightarrow -\infty} \frac{d}{\mu} \\
&= (\gamma+1) \lim_{\frac{\beta}{\alpha} \rightarrow -\infty} \frac{1}{\mu} \\
&= (\gamma+1) \lim_{\frac{\beta}{\alpha} \rightarrow -\infty} \frac{\alpha\sqrt{2} D_{-\gamma-1} \left(-\frac{\beta}{\alpha\sqrt{2}}\right)}{\gamma+1 D_{-\gamma-2} \left(-\frac{\beta}{\alpha\sqrt{2}}\right)} \\
&= \lim_{\frac{\beta}{\alpha} \rightarrow -\infty} \alpha\sqrt{2} \frac{D_{-\gamma-1} \left(-\frac{\beta}{\alpha\sqrt{2}}\right)}{D_{-\gamma-2} \left(-\frac{\beta}{\alpha\sqrt{2}}\right)} \left(D_v(z) = z D_{v-1}(z) - (v-1) D_{v-2}(z) \right) \\
&= \lim_{\frac{\beta}{\alpha} \rightarrow -\infty} \alpha\sqrt{2} \left(-\frac{\beta}{\alpha\sqrt{2}} + (\gamma+2) \frac{D_{-\gamma-3} \left(-\frac{\beta}{\alpha\sqrt{2}}\right)}{D_{-\gamma-2} \left(-\frac{\beta}{\alpha\sqrt{2}}\right)} \right) \\
&= -\beta.
\end{aligned}$$

Plugging these results into (15) yields

$$\begin{aligned}
KL_{\frac{\beta}{\alpha} \rightarrow -\infty}(q, p) &= (\gamma+1) \log(-\beta) - (\gamma+1) \left(\frac{\alpha^2(d+1)}{\beta^2} \right) - \log \left(\frac{(2\alpha^2)^{\frac{\gamma+1}{2}} e^{-\frac{\beta^2}{8\alpha^2}}}{D_{-\gamma-1} \left(-\frac{\beta}{\alpha\sqrt{2}}\right)} \right) \\
&= \log \left(\left(\frac{-\beta}{\alpha\sqrt{2}} \right)^{\gamma+1} \frac{D_{-\gamma-1} \left(-\frac{\beta}{\alpha\sqrt{2}}\right)}{e^{-\frac{\beta^2}{4(2\alpha^2)}}} \right) - (\gamma+1) \left(\frac{\alpha^2(d+1)}{\beta^2} \right) = 0,
\end{aligned}$$

since $\lim_{z \rightarrow \infty} \frac{D_{-v}(z)}{z^{-v} e^{-\frac{z^2}{4}}} = 1$

- **Asymptotic behaviour when $\frac{\beta}{\alpha} \rightarrow +\infty$ or $\gamma \rightarrow +\infty$:**

When $\frac{\beta}{\alpha} \rightarrow +\infty$ the Gamma-3p is approximated with a $\mathcal{N}(\mu, \sigma^2)$ distribution, with

$$\begin{aligned} \lim_{\frac{\beta}{\alpha} \rightarrow +\infty} \mu &= \lim_{\frac{\beta}{\alpha} \rightarrow +\infty} \frac{\gamma + 1}{\alpha\sqrt{2}} \frac{D_{-\gamma-2}\left(-\frac{\beta}{\alpha\sqrt{2}}\right)}{D_{-\gamma-1}\left(-\frac{\beta}{\alpha\sqrt{2}}\right)} \left(\lim_{x \rightarrow -\infty} v \frac{D_{-v-1}(z)}{D_{-v}(z)} = -z \right) \\ &= \frac{\beta}{2\alpha^2} \end{aligned} \quad (16)$$

and

$$\begin{aligned} \lim_{\frac{\beta}{\alpha} \rightarrow +\infty} \sigma^2 &= \lim_{\frac{\beta}{\alpha} \rightarrow +\infty} \frac{\gamma + 1^2}{2\alpha^2} \frac{D_{-\gamma-2}\left(-\frac{\beta}{\alpha\sqrt{2}}\right)}{D_{-\gamma-1}\left(-\frac{\beta}{\alpha\sqrt{2}}\right)} \left(\frac{\gamma + 2}{\gamma + 1} \frac{D_{-\gamma-3}\left(-\frac{\beta}{\alpha\sqrt{2}}\right)}{D_{-\gamma-2}\left(-\frac{\beta}{\alpha\sqrt{2}}\right)} - \frac{D_{-\gamma-2}\left(-\frac{\beta}{\alpha\sqrt{2}}\right)}{D_{-\gamma-1}\left(-\frac{\beta}{\alpha\sqrt{2}}\right)} \right) \\ &= \frac{1}{2\alpha^2}. \end{aligned} \quad (17)$$

Following Segura (2021), when $v \rightarrow \infty$ a sharp approximation for the ratio of Parabolic Cylinder functions is $v \frac{D_{-v-1}(z)}{D_{-v}(z)} \approx -z + \frac{1}{2}(z + \sqrt{z^2 + 4v - 2})$. Therefore, the mean and variance of the gaussian approximation become

$$\begin{aligned} \lim_{\gamma \rightarrow +\infty} \mu &= \lim_{\gamma \rightarrow +\infty} \frac{\gamma + 1}{\alpha\sqrt{2}} \frac{D_{-\gamma-2}\left(-\frac{\beta}{\alpha\sqrt{2}}\right)}{D_{-\gamma-1}\left(-\frac{\beta}{\alpha\sqrt{2}}\right)} \\ &= \frac{\beta}{4\alpha^2} + \frac{1}{\alpha\sqrt{8}} \sqrt{\frac{\beta^2}{2\alpha^2} + 4\gamma + 2} \end{aligned} \quad (18)$$

and

$$\begin{aligned} \lim_{\gamma \rightarrow +\infty} \sigma^2 &= \lim_{\gamma \rightarrow +\infty} \frac{\gamma + 1^2}{2\alpha^2} \frac{D_{-\gamma-2}\left(-\frac{\beta}{\alpha\sqrt{2}}\right)}{D_{-\gamma-1}\left(-\frac{\beta}{\alpha\sqrt{2}}\right)} \left(\frac{\gamma + 2}{\gamma + 1} \frac{D_{-\gamma-3}\left(-\frac{\beta}{\alpha\sqrt{2}}\right)}{D_{-\gamma-2}\left(-\frac{\beta}{\alpha\sqrt{2}}\right)} - \frac{D_{-\gamma-2}\left(-\frac{\beta}{\alpha\sqrt{2}}\right)}{D_{-\gamma-1}\left(-\frac{\beta}{\alpha\sqrt{2}}\right)} \right) \\ &= \frac{\gamma + 1}{4\alpha^2} \left(\frac{\beta}{\alpha\sqrt{2}} + \sqrt{\frac{\beta^2}{2\alpha^2} + 4\gamma + 6} \right) - \lim_{\gamma \rightarrow +\infty} \mu^2 \\ &= \frac{\gamma + 1}{4\alpha^2} \left(\frac{\beta}{\alpha\sqrt{2}} + \sqrt{\frac{\beta^2}{2\alpha^2} + 4\gamma + 6} \right) - \left(\frac{\beta}{4\alpha^2} + \frac{1}{\alpha\sqrt{8}} \sqrt{\frac{\beta^2}{2\alpha^2} + 4\gamma + 2} \right)^2. \end{aligned} \quad (19)$$

Tables 5 and 6 show the KL divergence for increasing values of the ratio β/α and γ . The integral is numerically approximated with the command `KLD` from package `LaplacesDemon` for software R. The approximated KL divergence is evaluated over the interval $(\mu - 5\sigma, \mu + 5\sigma)$. Values of the parameters higher than those shown in the table 5 give overflow problems.

The results in the tables below depend only on the values of γ and the ratio β/α , that is, for different values of α the KL divergence between $q \sim \mathcal{G}_{3p}(\gamma, \alpha, \beta)$ and $p \sim \mathcal{N}(\mu, \sigma^2)$ does not change. The sequence of KL divergence is always decreasing in Table 6, for both $\text{KL}(q||p)$ and $\text{KL}(p||q)$. In Table 5 the sequence is decreasing only for $\text{KL}(p||q)$, however the mean between the two is decreasing.

KL	$\frac{\beta}{\alpha} = 0.002$	$\frac{\beta}{\alpha} = 0.2$	$\frac{\beta}{\alpha} = 0.5$	$\frac{\beta}{\alpha} = 1$	$\frac{\beta}{\alpha} = 3$	$\frac{\beta}{\alpha} = 5$	$\frac{\beta}{\alpha} = 8$	$\frac{\beta}{\alpha} = 0.002$	$\frac{\beta}{\alpha} = 0.2$	$\frac{\beta}{\alpha} = 0.5$	$\frac{\beta}{\alpha} = 1$	$\frac{\beta}{\alpha} = 3$	$\frac{\beta}{\alpha} = 5$	$\frac{\beta}{\alpha} = 8$
$\gamma = 1$	0.284	0.273	0.257	0.227	0.105	0.041	0.016	0.411	0.394	0.372	0.329	0.139	0.047	0.016
$\gamma = 3$	1.206	1.164	1.100	0.983	0.545	0.281	0.127	2.365	2.288	2.153	1.906	0.886	0.355	0.139
$\gamma = 5$	2.185	2.115	2.007	1.820	1.104	0.636	0.318	5.032	4.858	4.577	4.064	1.992	0.871	0.366
$\gamma = 10$	4.633	4.505	4.319	3.995	2.736	1.810	1.038	13.207	12.743	12.057	10.804	5.698	2.811	1.303
$\gamma = 15$	6.875	6.740	6.516	6.124	4.501	3.206	1.990	22.597	21.884	20.721	18.653	10.295	5.419	2.672
$\gamma = 30$	10.882	10.839	10.751	10.537	9.160	7.568	5.517	53.998	52.316	49.941	45.377	27.042	15.766	8.645
$\gamma = 50$	12.710	12.739	12.749	12.708	12.090	11.137	9.542	97.765	95.186	90.974	83.411	52.121	32.489	19.310
$\gamma = 100$	14.162	14.225	14.278	14.349	14.163	13.755	13.110	208.476	203.439	195.323	180.003	117.316	77.428	49.973

Table 5: KL divergence when β/α increases: $\text{KL}(q||p)$ (left) and $\text{KL}(p||q)$ (right) where $q \sim \mathcal{G}_{3p}(\gamma, \alpha, \beta)$ and $p \sim \mathcal{N}(\mu, \sigma^2)$, with μ and σ^2 computed as in (16)-(17).

KL	$\frac{\beta}{\alpha} = 0.002$	$\frac{\beta}{\alpha} = 0.2$	$\frac{\beta}{\alpha} = 0.5$	$\frac{\beta}{\alpha} = 1$	$\frac{\beta}{\alpha} = 3$	$\frac{\beta}{\alpha} = 5$	$\frac{\beta}{\alpha} = 8$	$\frac{\beta}{\alpha} = 0.002$	$\frac{\beta}{\alpha} = 0.2$	$\frac{\beta}{\alpha} = 0.5$	$\frac{\beta}{\alpha} = 1$	$\frac{\beta}{\alpha} = 3$	$\frac{\beta}{\alpha} = 5$	$\frac{\beta}{\alpha} = 8$
$\gamma = 1$	0.022	0.021	0.018	0.016	0.011	0.007	0.004	0.023	0.022	0.020	0.017	0.010	0.007	0.003
$\gamma = 3$	0.015	0.013	0.012	0.010	0.005	0.004	0.002	0.025	0.023	0.020	0.015	0.005	0.004	0.002
$\gamma = 5$	0.010	0.009	0.008	0.006	0.003	0.002	0.002	0.016	0.015	0.013	0.010	0.004	0.002	0.002
$\gamma = 10$	0.005	0.004	0.004	0.003	0.002	0.001	0.001	0.006	0.006	0.005	0.004	0.002	0.001	0.001
$\gamma = 15$	0.003	0.003	0.003	0.002	0.001	0.001	< 0.001	0.003	0.003	0.003	0.003	0.001	0.001	< 0.001
$\gamma = 30$	0.001	0.001	0.001	0.001	< 0.001	< 0.001	< 0.001	0.002	0.001	0.001	0.001	< 0.001	< 0.001	< 0.001
$\gamma = 50$	< 0.001	< 0.001	< 0.001	< 0.001	< 0.001	< 0.001	< 0.001	< 0.001	< 0.001	< 0.001	< 0.001	< 0.001	< 0.001	< 0.001
$\gamma = 100$	< 0.001	< 0.001	< 0.001	< 0.001	< 0.001	< 0.001	< 0.001	< 0.001	< 0.001	< 0.001	< 0.001	< 0.001	< 0.001	< 0.001

Table 6: KL divergence when γ increases: $\text{KL}(q||p)$ (left) and $\text{KL}(p||q)$ (right) where $q \sim \mathcal{G}_{3p}(\gamma, \alpha, \beta)$ and $p \sim \mathcal{N}(\mu, \sigma^2)$, with μ and σ^2 computed as in (18)-(19).

Supplementary material: Inference of multiple high-dimensional networks with the Graphical Horseshoe prior

Claudio Busatto

Department of Statistics, Computer Science, Applications "G. Parenti",
University of Florence, Florence, Italy

and

Francesco Claudio Stingo

Department of Statistics, Computer Science, Applications "G. Parenti",
University of Florence, Florence, Italy

February 14, 2023

This supplementary provides the pseudo-code for mGHS algorithm and additional graphs and tables for the analysis of the bike-sharing dataset in Section 7. In particular, Appendix B shows the estimated networks for each group across the years for both GHS and mGHS and the analysis of the convergence of mGHS algorithm.

A Pseudo-code for mGHS algorithm

Algorithm 1: multiple Graphical Horseshoe algorithm

1 Input: $\mathbf{S}_1, \dots, \mathbf{S}_K \in \mathbb{R}^{p \times p}$, $K, p, B, bn \in \mathbb{N}$, $\mathbf{n} \in \mathbb{N}^K$;
2 set $\boldsymbol{\Omega}_k = \mathbf{I}_p$, $\boldsymbol{\Sigma}_k = \mathbf{I}_p$, $\boldsymbol{\Lambda}_k = \mathbf{1}_{p \times p}$, $\boldsymbol{\eta}_k = \mathbf{1}_{p \times p}$, $\boldsymbol{\tau} = \mathbf{1}_K$, $\boldsymbol{\zeta} = \mathbf{1}_K$, $\mathbf{R} = \mathbf{I}_K$ and $\boldsymbol{\mu} = \mathbf{0}_K$;
3 for $b = 1$ to B **do**
4 **for** $k = 1$ to K **do**
5 **for** $j = 1$ to p **do**
6 compute $\mathbf{t}_{j,k} := \{t_{j,k}^i = \mathbf{r}_k^\top \mathbf{R}_{-k}^{-1} \boldsymbol{\Delta}_{ij,-k}^{-1} \boldsymbol{\omega}_{ij}^{-k}, i = 1, \dots, p, i \neq j\}$;
7 compute $\mathbf{m}_{j,k} := \{m_{j,k}^i = t_{j,k}^i \sqrt{\tau_k \lambda_{ij}^k}, i = 1, \dots, p, i \neq j\}$;
8 compute $\mathbf{D}_{j,k} := \{D_{j,k}^{ii} = \mu_k \tau_k \lambda_{ij}^k, i = 1, \dots, p, i \neq j\}$;
9 compute $\mathbf{O}_{j,k} = \boldsymbol{\Sigma}_{-j}^k - \boldsymbol{\sigma}_j^k \left(\boldsymbol{\sigma}_j^k / \sigma_{jj}^k \right)^\top$ and $\mathbf{W}_{j,k} = \mathbf{D}_{j,k} + s_{jj}^k \mathbf{O}_{j,k}$;
10 sample $\gamma_{jj}^k \sim \mathcal{IG}(n_k/2 + 1, s_{jj}^k/2)$;
11 sample $\mathbf{v}_{j,k} \sim \mathcal{N}_{p-1}(\mathbf{W}_{j,k}^{-1} (\mathbf{D}_{j,k}^{-1} \mathbf{m}_{j,k} - \mathbf{s}_{-j}^k), \mathbf{W}_{j,k}^{-1})$;
12 sample $\mathbf{e}_{j,k} := \{e_{j,k}^i \sim \mathcal{IG}(1, 1 + 1/l_{j,k}^i), i = 1, \dots, p, i \neq j\}$;
13 sample $\mathbf{l}_{j,k} := \left\{ l_{j,k}^i \sim \mathcal{G}_{3p} \left(1, \alpha_{\lambda_{ij,k}}, \beta_{\lambda_{ij,k}} \right)^{-2}, i = 1, \dots, p, i \neq j \right\}$, where $\alpha_{\lambda_{ij,k}} = \left(\frac{v_i^2}{2\tau_k \mu_k} + \frac{1}{\eta_{ij}^k} \right)^{1/2}$ and
 $\beta_{\lambda_{ij,k}} = \frac{v_i}{\sqrt{\tau_k \mu_k}} t_{j,k}^i$;
14 set $\boldsymbol{\Sigma}_{-j}^k = \mathbf{O}_{j,k} + \mathbf{O}_{j,k} \mathbf{v}_{j,k} \mathbf{v}_{j,k}^\top \mathbf{O}_{j,k} / \gamma_{jj}^k$, $\boldsymbol{\sigma}_j^k = -\mathbf{O}_{j,k} \mathbf{v}_{j,k} / \gamma_{jj}^k$, $\sigma_{jj}^k = 1/\gamma_{jj}^k$, $\boldsymbol{\omega}_j^k = \mathbf{v}_{j,k}$,
 $\boldsymbol{\omega}_{jj}^k = \gamma_{jj}^k + \mathbf{v}_{j,k}^\top \mathbf{O}_{j,k} \mathbf{v}_{j,k}$, $\boldsymbol{\lambda}_j^k = \mathbf{l}_{j,k}$ and $\boldsymbol{\eta}_j^k = \mathbf{e}_{j,k}$;
15 **end for**
16 **end for**
17 compute $\mathbf{T}_k := \{T_k^{ij} = \mathbf{r}_k^\top \mathbf{R}_{-k}^{-1} \boldsymbol{\Delta}_{ij,-k}^{-1} \boldsymbol{\omega}_{ij}^{-k}, k = 1, \dots, K, j = 2, \dots, p, i < j\}$;
18 sample $\boldsymbol{\tau} := \left\{ \tau_k \sim \mathcal{G}_{3p}(p(p-1)/2, \alpha_{\tau_k}, \beta_{\tau_k})^{-2}, k = 1, \dots, K \right\}$, where $\alpha_{\tau_k} = \left(\frac{1}{\zeta_k} + \sum_{i < j} \frac{(\omega_{ij}^k)^2}{2\lambda_{ij}^k \mu_k} \right)^{1/2}$ and
 $\beta_{\tau_k} = \sum_{i < j} \frac{\omega_{ij}^k}{\sqrt{\lambda_{ij}^k \mu_k}} \mathbf{T}_k^{ij}$;
19 sample $\boldsymbol{\zeta} := \{\zeta_k \sim \mathcal{IG}(1, 1 + 1/\tau_k), k = 1, \dots, K\}$;
20 sample $\mathbf{R}_* = \text{diag}(\boldsymbol{\Psi})^{-1/2} \boldsymbol{\Psi} \text{diag}(\boldsymbol{\Psi})^{-1/2}$, where $\boldsymbol{\Psi} \sim \mathcal{IW}(p(p-1)/2, \mathbf{H})$ and
 $\mathbf{H} := \left\{ H_{ij} = \sum_{k=1}^K \left(\sum_{i < j} \omega_{ij}^k \right)^{-1/2} \frac{\omega_{ij}^k}{\sqrt{\tau_k \lambda_{ij}^k}} \right\}$;
21 **if** $\mathcal{U}(0, 1) < e^{(K+1)/2(\log |\mathbf{R}_*| - \log |\mathbf{R}|)}$ **then** set $\mathbf{R} = \mathbf{R}_*$ and compute $\boldsymbol{\mu} := \left\{ \mu_k = 1 - \mathbf{r}_k^\top \mathbf{R}_{-k}^{-1} \mathbf{r}_k, k = 1, \dots, K \right\}$;
22 **end for**
23 **return** $\boldsymbol{\Omega}_1, \dots, \boldsymbol{\Omega}_K, \boldsymbol{\Lambda}_1, \dots, \boldsymbol{\Lambda}_K, \boldsymbol{\tau}$ and \mathbf{R} ;

B Bike-sharing dataset: convergence analysis and estimated graph for each group

Here we provide the analysis of the convergence of mGHS algorithm. We run $M = 4$ chains by starting from different starting points for a post-burnin period of 5000 iterations. The convergence of the algorithm is studied in Figure 1 by estimating the potential scale reduction factor for parameters ω_{ij}^k , $i = 1, \dots, 239$, $j > i$, $k = 1, \dots, 6$, whereas the post-burnin trace of the joint posterior distribution of the chains is shown in Figure 2. In Figure 1, the percentage of values that lies in the interval $[1.0, 1.2]$ is greater than 99% for each group, with the only exception of the group members in 2017 for which this percentage is 98%. The estimated bike-sharing networks for each group with both mGHS and GHS are shown in Figure 3 and 4, respectively, where black edges denote those edges included in all three years for both member and casual users.

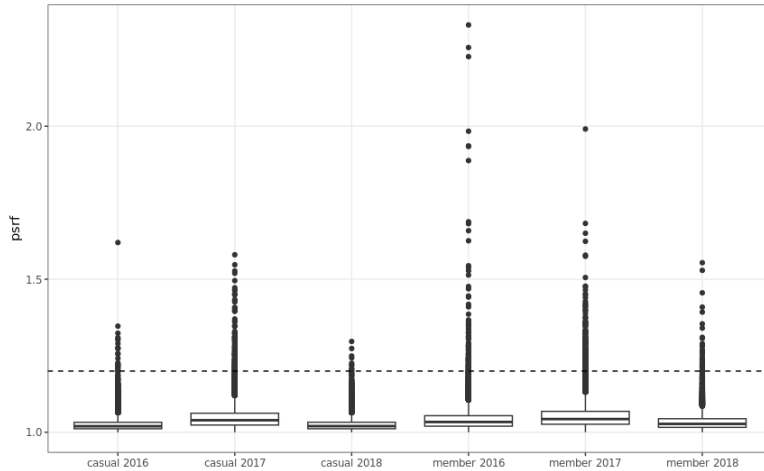


Figure 1: Distribution of the estimated potential scale reduction factors computed over a post-burning period of 5000 updates for parameters ω_{ij}^k across 4 replications. Optimal values of the index should lie under the dotted line ($y = 1.2$).

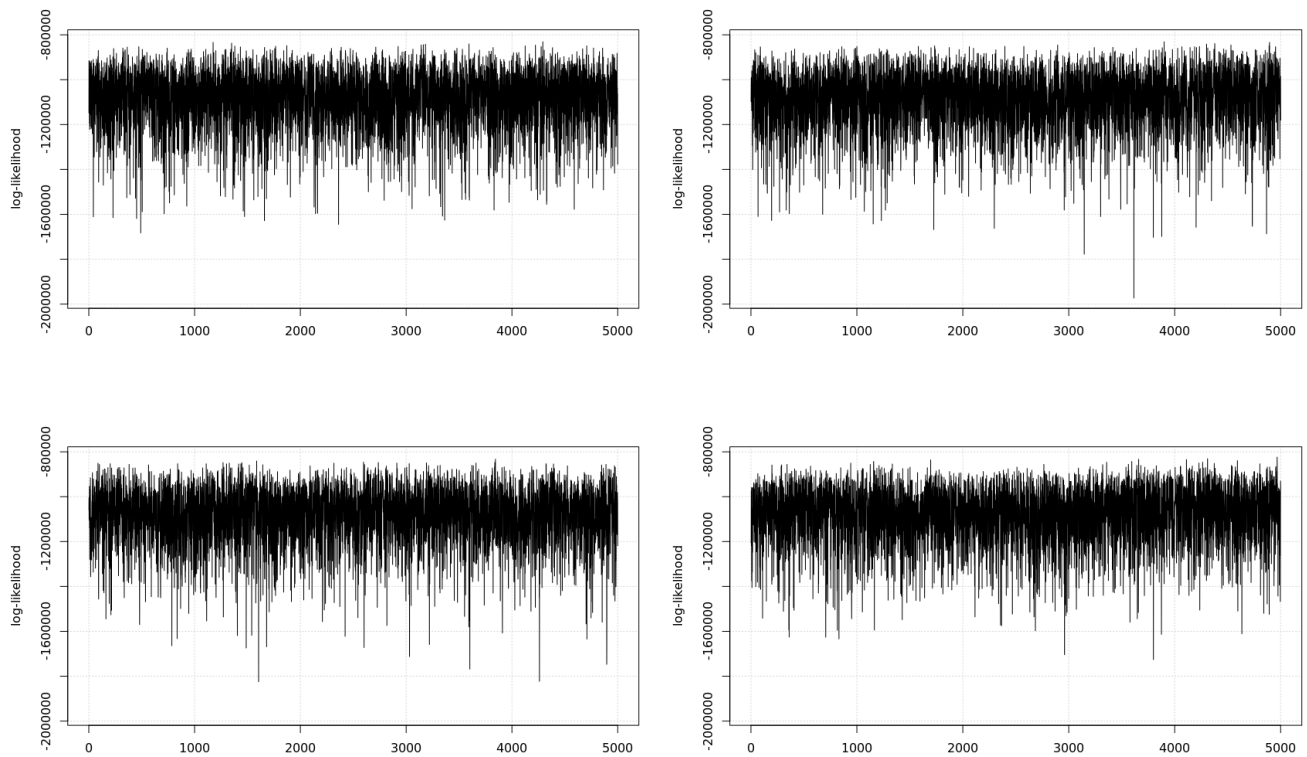


Figure 2: Post-burnin trace of the joint posterior distribution of the 4 chains.

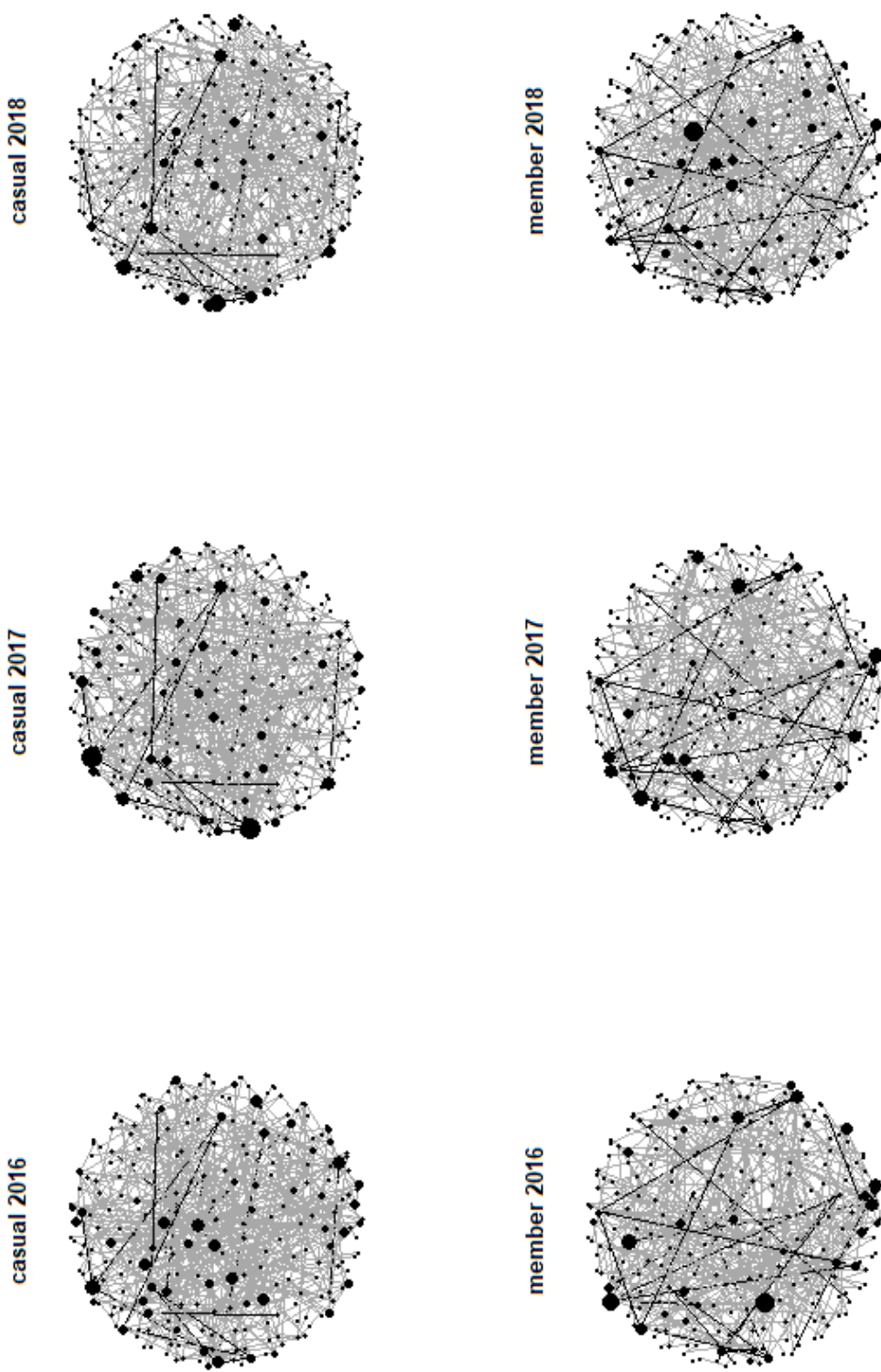


Figure 3: Estimated graph by mGHS for each group; Black edges denote those edges included in all three years for both member and casual users and the size of the nodes depends on the number of edges associated to the related station.

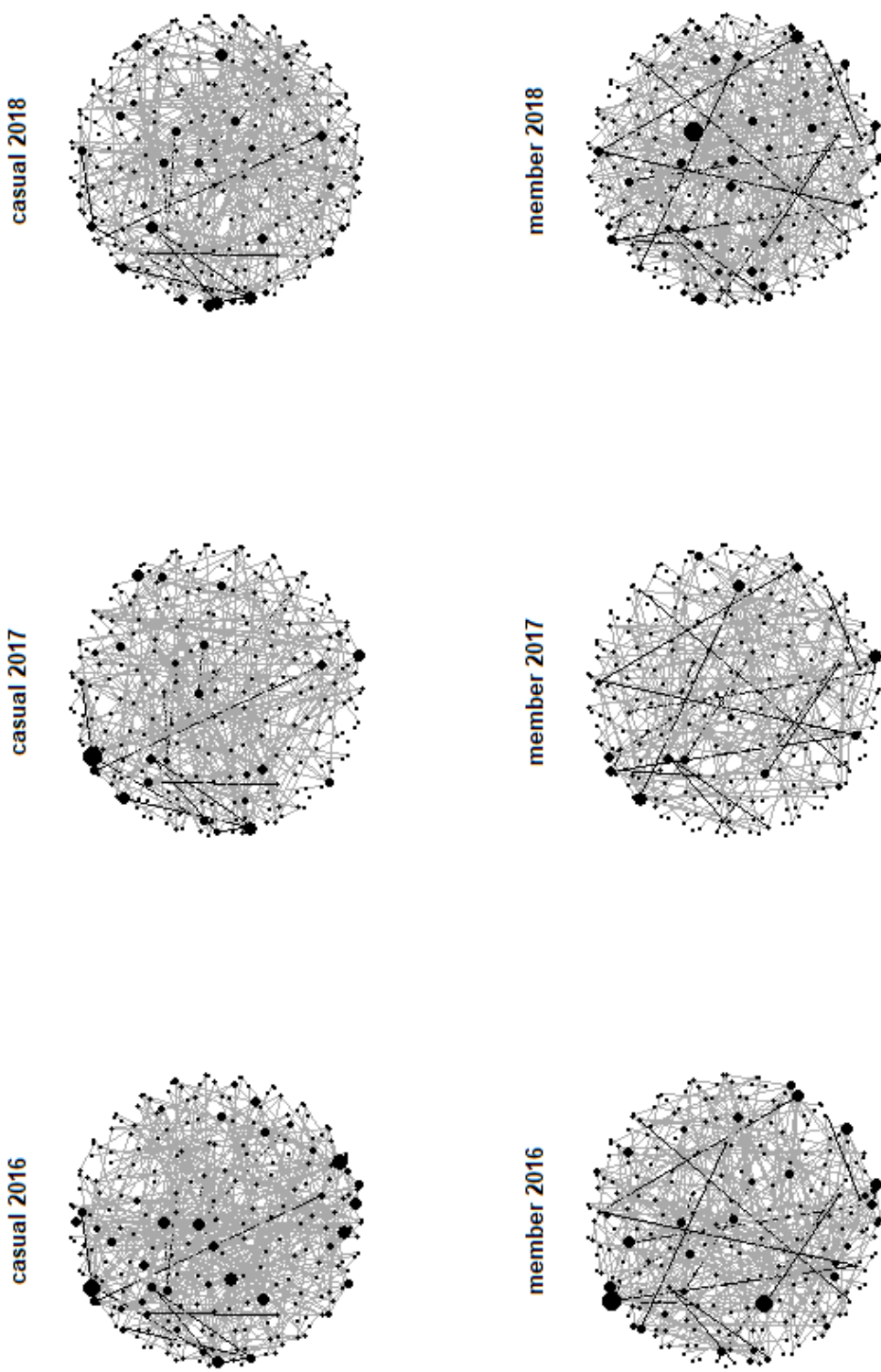


Figure 4: Estimated graph by GHS for each group; black edges denote those edges included in all three years for both member and casual users and the size of the nodes depends on the number of edges associated to the related station.